

# Computing Barycentres of Measures for Generic Transport Costs

Eloi Tanguy<sup>1</sup>, Julie Delon<sup>1</sup>, and Nathaël Gozlan<sup>1</sup>

<sup>1</sup>Université Paris Cité, CNRS, MAP5, F-75006 Paris, France

13th February 2026

## Abstract

Wasserstein barycentres represent average distributions between multiple probability measures for the Wasserstein distance. The numerical computation of Wasserstein barycentres is notoriously challenging. A common approach is to use Sinkhorn iterations, where an entropic regularisation term is introduced to make the problem more manageable. Another approach involves using fixed-point methods, akin to those employed for computing Fréchet means on manifolds. The convergence of such methods for 2-Wasserstein barycentres, specifically with a quadratic cost function and absolutely continuous measures, was studied by Alvarez-Esteban et al. in [Álv+16]. In this paper, we delve into the main ideas behind this fixed-point method and explore how it can be generalised to accommodate more diverse transport costs and generic probability measures, thereby extending its applicability to a broader range of problems. We show convergence results for this approach and illustrate its numerical behaviour on several barycentre problems.

## Table of Contents

<b>1</b>	<b>Introduction</b>	<b>2</b>
1.1	Related Works and Motivation . . . . .	2
1.2	Contributions and Outline . . . . .	4
<b>2</b>	<b>Lifting Ground Barycentres to Measures</b>	<b>4</b>
<b>3</b>	<b>A Fixed-Point Algorithm</b>	<b>6</b>
3.1	Algorithm Definition . . . . .	6
3.2	Convergence of Fixed-Point Iterations . . . . .	8
3.3	Expression of the Iterates when the Plans are Maps . . . . .	15
3.4	The Particular Case of Conditionally Independent Couplings . . . . .	16
<b>4</b>	<b>Focus on the Discrete Case</b>	<b>17</b>
4.1	Discrete Expression and Algorithms . . . . .	17
4.2	Correspondence of Gradient Descent with Fixed-Point Iterations . . . . .	20
4.3	Discrete Uniqueness Discussion . . . . .	22
4.4	Application to Gaussian Mixture Model Barycentres . . . . .	23
<b>5</b>	<b>Numerical Illustrations</b>	<b>24</b>

arXiv:2501.04016v3 [math.NA] 27 Mar 2026

5.1	Toy Example for Barycentre Computation	25
5.2	Illustration with Norm Powers	25
5.3	Study of the Support Size of Iterates of $G$	27
5.4	Comparison with the Multi-Marginal Formulation	28
5.5	Generalised Wasserstein Barycentre Computation	31
5.6	Non-linear Generalised Wasserstein Barycentre Computation	31
5.7	Gaussian Mixture Model Barycentres	32
5.8	Colour Transfer on a Barycentre of Colour Distributions	33

# 1 Introduction

## 1.1 Related Works and Motivation

Wasserstein barycentres represent a powerful concept in Optimal Transport theory, enabling the computation of average distributions between multiple probability measures. These barycentres preserve the geometric structure of the underlying distributions, making them particularly suited for machine learning tasks. They have proven useful in numerous applications, including image processing [Rab+12], computer graphics [Sol+15; BPC16], statistics [BCP19], domain adaptation [MM21], generative modelling [Kor+22], fairness in machine learning [Gor+19] or model selection in Bayesian learning [Bac+22]. Wasserstein barycentres are also at the core of clustering methods such as K-means, to define centroids in spaces of probability measures [Ho+17; Mi+18].

The classical notion of barycentre refers to the weighted average of a set of points  $(x_k)$  with positive weights  $(\lambda_k)$  summing to 1, in a metric space  $(E, d)$ . Formally, a barycentre  $\bar{x}$  is a point that minimises the weighted sum of (typically squared) distances:

$$\bar{x} \in \operatorname{argmin}_{x \in E} \sum_{k=1}^K \lambda_k d^2(x, x_k).$$

This concept can be extended to the space of probability measures, where  $d$  can be replaced for instance by a transportation cost  $\mathcal{T}_c$ . We remind that for two probability measures  $\mu$  and  $\nu$  on metric spaces  $(\mathcal{X}, d_{\mathcal{X}})$  and  $(\mathcal{Y}, d_{\mathcal{Y}})$ , and a cost function  $c : \mathcal{X} \times \mathcal{Y} \rightarrow \mathbb{R}_+$ , the optimal transport cost between  $\mu$  and  $\nu$  for the ground cost  $c$  is defined as

$$\mathcal{T}_c(\mu, \nu) = \inf_{\pi \in \Pi(\mu, \nu)} \int_{\mathcal{X} \times \mathcal{Y}} c d\pi,$$

where  $\Pi(\mu, \nu)$  is the set of probability measures on  $\mathcal{X} \times \mathcal{Y}$  with marginals  $\mu$  and  $\nu$ . Considering  $K$  different cost functions  $c_k$ , the barycentre problem can be written in this setting as

$$\bar{\mu} \in \operatorname{argmin}_{\mu} \sum_{k=1}^K \lambda_k \mathcal{T}_{c_k}(\mu, \nu_k). \quad (1)$$

When  $(\mathcal{X}, d_{\mathcal{X}}) = (\mathcal{Y}, d_{\mathcal{Y}})$  is a Polish space and  $c = d_{\mathcal{X}}^p$  with  $p \geq 1$ ,  $W_p(\mu, \nu) := (\mathcal{T}_{d^p}(\mu, \nu))^{\frac{1}{p}}$  defines a distance between probability measures (with finite moment of order  $p$ ), called  $p$ -Wasserstein distance. In this case, the barycentre  $\bar{\mu}$  defined above is called a Wasserstein barycentre. Generalisation to a barycentre of a probability measure on  $\mathcal{P}(\mathcal{X})$  and the consistency of their discrete approximations is also studied by several authors [AC17].

The theoretical analysis of Wasserstein barycentres begins with the foundational work by Carlier and Ekeland [CE10], who studied the existence, uniqueness and dual formulations for

barycentre problems with generic continuous cost functions. Subsequent work by [AC11] re-established the existence and dual formulations of such barycentres for the quadratic Wasserstein distance  $W_2$  on Euclidean spaces, and showed uniqueness under the hypothesis that one of the original measures is absolutely continuous. More recent studies have broadened these results: [CCE24] extended the theoretical analysis to Wasserstein medians ( $W_1$ ), studying their stability properties, and investigated dual and multi-marginal formulations. [BFR24b] further extended the framework to  $W_p$  distances for  $p > 1$ , proving existence and uniqueness of barycentres for absolutely continuous measures on  $\mathbb{R}^d$ . A follow-up study by [BFR24a] analysed the general case for strictly convex and  $\mathcal{C}^2$  cost functions with non-degenerate Hessian.

From a computational perspective, calculating Wasserstein barycentres is known to be a highly challenging problem, classified as NP-hard. According to [AB21], although polynomial-time algorithms exist for computing Wasserstein barycentres with a fixed number of points, their computational complexity scales exponentially with respect to the dimension of the space, or with respect to the number of marginals. This makes direct computation infeasible for high-dimensional problems or large sets of distributions, which are common in practical applications.

To tackle these computational challenges, several approximate methods have been developed for Wasserstein barycentres. The first paper to propose an algorithmic solution for computing these barycentres was [Rab+12], which computed Sliced Wasserstein barycentres through a gradient descent approach. This method leveraged the sliced Wasserstein distance to achieve an efficient approximation, significantly simplifying computations.

A natural approach to develop easily computable approximations of such barycentres is to replace transport costs  $\mathcal{T}_c$  by regularised versions

$$\mathcal{T}_{c,\varepsilon}(\mu, \nu) = \inf_{\pi \in \Pi(\mu, \nu)} \int_{\mathcal{X} \times \mathcal{Y}} c d\pi + \varepsilon \text{KL}(\pi | \mu \otimes \nu),$$

as proposed in [CD14]. When the support of the distributions and barycentre is fixed (a grid for instance), the problem can be rewritten as a KL projection problem and the so-called entropic barycentre can be computed efficiently with a modified version of Sinkhorn's algorithm [Ben+15; PC19].

In order to deal with distributions without imposed support a second approach also described in [CD14] relies on a fixed-point algorithm inspired by the computation of Fréchet means on manifolds. Each step of this fixed point approach consists in replacing the current barycentre  $\mu$  by its image measure by the map  $\sum_{k=1}^K \lambda_k T_k$ , where the  $T_k$  are optimal maps between  $\mu$  and  $\nu_k$  (assuming these maps exist). The authors of [Álv+16] were the first to establish a rigorous proof of convergence for this fixed-point approach in the case of absolutely continuous measures  $\nu_k$ : more precisely, they proved convergence of a subsequence to a fixed point and showed that if the fixed point is unique, it is indeed a barycentre. Their study focuses specifically on the case of  $W_2$  barycentres, with applications demonstrated mainly on Gaussian measures. Although their proof is only provided for absolutely continuous measures, this fixed point approach is frequently used for discrete measures and probably the baseline free-support method provided in numerical optimal transport libraries [Fla+21]. Building on the same ideas as [Álv+16], the author of [Lin23] extends the investigation of the fixed point algorithm for discrete measures on  $\mathbb{R}^d$ , limited to just one single iteration, and deriving a worst-case error bound in the  $W_2$  and  $W_1$  settings. The iterative solver of [Álv+16] has also been extended in high dimensional settings by [Kor+22], which use a neural solver for computing the optimal maps  $T_k$ .

In closely related directions, several other approaches have been proposed to compute Wasserstein barycentres over Riemannian manifolds [KP17], or Gromov-Wasserstein barycentres [BB25; BBS23] and the approach we develop in this paper share similarities with [BB25].

## 1.2 Contributions and Outline

In this paper, we develop a fixed-point approach to compute barycentres between probability measures for generic transport costs, i.e. solutions of the optimisation problem (1). Our only hypotheses are that we work on compact spaces, and that the ground costs  $c_k$  are continuous and such that  $\operatorname{argmin}_x \sum_{k=1}^K \lambda_k c_k(x, x_k)$  is uniquely defined. In particular, we do not assume existence of optimal transport maps between  $\mu$  and the  $\nu_k$ , and we do not assume anything on the probability measures  $\mu$  and  $\nu_k$ . We propose an iterative fixed-point algorithm generalising [Álv+16] in this generic case. We show that the sequences generated by this algorithm have converging sub-sequences, that limits must be fixed-points of a certain mapping  $G$ , and that a barycentre for (1) is also a fixed point of  $G$ .

Numerically, we show that our approach specifically allows to extend the recent definition of generalised Wasserstein barycentres presented in [DGS21], notably by considering non-linear functions between the ambient space and the subspaces of measures  $\nu_k$ . It also enables efficient computation of barycentres for the mixture Wasserstein metric [DD20], which until now were calculated using their multi-marginal equivalent formulation.

The paper is organised as follows. In Section 2, we introduce a novel notion of Optimal Transport barycentres in a certain space between measures  $\nu_k$  on potentially different spaces for generic costs  $c_k$ . In Section 3, we propose a fixed-point algorithm which generalises [Álv+16] and converges to solutions (in a certain sense). We re-write the problem in a discrete setting in Section 4 and illustrate our method in Section 5 on several numerical examples, providing a publicly available Python toolkit.

## 2 Lifting Ground Barycentres to Measures

We work with probability measures  $\nu_k$  on compact metric spaces  $(\mathcal{Y}_k, d_{\mathcal{Y}_k})_{k \in [1, K]}$ ,<sup>1</sup> of which we will seek a “barycentre”  $\mu$  in a compact metric space  $(\mathcal{X}, d_{\mathcal{X}})$ . To compare a measure  $\nu_k \in \mathcal{P}(\mathcal{Y}_k)$  and  $\mu \in \mathcal{P}(\mathcal{X})$  we consider continuous cost functions  $c_k : \mathcal{X} \times \mathcal{Y}_k \rightarrow \mathbb{R}_+$ . A barycentre will be a minimiser of the sum of the transport costs with respect to the measure  $\nu_k$ , leading to the following energy for a measure  $\mu \in \mathcal{P}(\mathcal{X})$ :

$$V(\mu) := \sum_{k=1}^K \mathcal{T}_{c_k}(\mu, \nu_k), \quad (2)$$

hence our minimisation problem reads

$$\operatorname{argmin}_{\mu \in \mathcal{P}(\mathcal{X})} V(\mu). \quad (3)$$

Note that to introduce barycentre weights  $\lambda_k$ , it suffices to replace  $c_k$  with  $\lambda_k c_k$ , which allows us to include weights in the costs and alleviate notation. We summarise our standing assumptions on the spaces and costs in Assumption 1:

**Assumption 1.** *The metric spaces  $(\mathcal{X}, d_{\mathcal{X}})$  and  $(\mathcal{Y}_k, d_{\mathcal{Y}_k})$  are compact, and the costs  $c_k : \mathcal{X} \times \mathcal{Y}_k \rightarrow \mathbb{R}_+$  are continuous.*

Existence of solutions for Problem (3) was established by [CE10, Proposition 2] under Assumption 1.

<sup>1</sup>where for  $a, b \in \mathbb{N}$ ,  $\llbracket a, b \rrbracket$  denotes the set  $\{a, a+1, \dots, b\}$ .

**Remark 2.1.** Uniqueness was proven in [CE10, Proposition 4] if, essentially, for at least one  $k$ , the problem  $\mathcal{T}_{c_k}(\mu, \nu_k)$  has a Monge solution, for which they assume that each  $\nu_k$  is absolutely continuous on  $\mathcal{Y}_k = \bar{\Omega}$  with  $\Omega$  an open and bounded subset of  $\mathbb{R}^d$  with  $\nu_k(\partial\Omega) = 0$ . They also assume that the costs  $c_k(\cdot, y)$  are Lipschitz with a uniform constant  $L$  and that  $c_k$  verifies the Twist condition:  $c_k(\cdot, y)$  is differentiable, with  $\partial_x c_k(x, \cdot)$  injective.

The definition of a barycentre between measures  $\nu_k$  can be seen as a lifting of a notion of barycentre within  $\mathcal{X}$  of points  $(y_1, \dots, y_K) \in \mathcal{Y}_1 \times \dots \times \mathcal{Y}_K$ . To give mathematical meaning to this intuition and to our method, we will make the following assumption throughout the paper:

**Assumption 2.** For all  $(y_1, \dots, y_K) \in \mathcal{Y}_1 \times \dots \times \mathcal{Y}_K$ , the set  $\operatorname{argmin}_{x \in \mathcal{X}} \sum_{k=1}^K c_k(x, y_k)$  has a unique element.

The uniqueness of the optimisation problem in Assumption 2 allows us to introduce the ground barycentre function  $B$ :

$$B : \begin{cases} \mathcal{Y}_1 \times \dots \times \mathcal{Y}_K & \longrightarrow \\ (y_1, \dots, y_K) & \longmapsto \operatorname{argmin}_{x \in \mathcal{X}} \sum_{k=1}^K c_k(x, y_k). \end{cases} \quad (4)$$

For example, in the case  $\mathcal{X} = \mathcal{Y}_1 = \dots = \mathcal{Y}_K = \mathbb{R}^d$ , with  $c_k(x, y_k) = \|x - y_k\|_2^2$ , the ground barycentre function  $B$  is the standard Euclidean barycentre:  $B(y_1, \dots, y_K) = \frac{1}{K} \sum_{k=1}^K y_k$ . For convenience, we introduce  $\mathcal{Y} := \prod_k \mathcal{Y}_k$ , equipped with the product distance, with the notation  $Y := (y_1, \dots, y_K)$  for an element of  $\mathcal{Y}$ , as well as the total cost function:

$$C := \begin{cases} \mathcal{X} \times \mathcal{Y} & \longrightarrow \mathbb{R}_+ \\ (x, y_1, \dots, y_K) & \longmapsto \sum_{k=1}^K c_k(x, y_k) \end{cases}. \quad (5)$$

Equipped with these convenient notations, we can write the multi-marginal formulation of our barycentre problem:

$$\operatorname{argmin}_{\pi \in \Pi(\nu_1, \dots, \nu_K)} \int_{\mathcal{Y}} C(B(Y), Y) d\pi(Y). \quad (6)$$

The barycentre problem defined in Eq. (3) is related to the multi-marginal formulation through the following equation, due to [CE10, Proposition 3.3]:

$$\operatorname{argmin}_{\mu \in \mathcal{P}(\mathcal{X})} V(\mu) = B \# \operatorname{argmin}_{\pi \in \Pi(\nu_1, \dots, \nu_K)} \int_{\mathcal{Y}} C(B(Y), Y) d\pi(Y), \quad (7)$$

where  $\#$  denotes the push-forward operator:  $f \# \mu := \operatorname{Law}_{X \sim \mu}[f(X)]$ . The following technical result uses the continuity of the  $c_k$  and Assumption 2 to show that  $B$  is continuous.

**Lemma 2.2.** The function  $B : \mathcal{Y} \longrightarrow \mathcal{X}$  defined in Eq. (4) is continuous.

**Proof.** The proof uses standard compactness arguments, showing that for  $Y_n \xrightarrow[n \rightarrow +\infty]{} Y \in \mathcal{Y}$ ,  $(B(Y_n))$  can only have  $B(Y)$  as a subsequential limit.  $\square$

Another important technical result is the regularity of transport costs, which we will use repeatedly. We gather well-known results in Lemma 2.3.

**Lemma 2.3.** *Consider  $E, F$  compact metric spaces and let  $c : E \times F \rightarrow \mathbb{R}_+$  a measurable cost function. The optimal transport cost  $\mathcal{T}_c$  has the following regularity for the weak convergence of measures depending on  $c$ :*

1. *If  $c$  is lower-semi-continuous, then  $\mathcal{T}_c$  is lower-semi-continuous.*
2. *If  $c$  is continuous, then  $\mathcal{T}_c$  is continuous.*
3. *If  $E = F$  and  $c$  is l.s.c. with  $c(x, y) = 0 \implies x = y$ , then  $\mathcal{T}_c(\mu, \nu) = 0 \implies \mu = \nu$ .*

**Proof.** Regarding item 1), by [San15, Theorem 1.42], Kantorovich duality holds for  $c$  l.s.c. and thus  $\mathcal{T}_c$  can be written as a supremum of l.s.c. functions, hence is l.s.c.. For item 2), the result is verbatim [San15, Theorem 1.51]. For item 3), if  $\mathcal{T}_c(\mu, \nu) = 0$  then there exists  $\pi \in \Pi(\mu, \nu)$  such that  $\int_{E^2} c(x, y) d\pi(x, y) = 0$  (existence follows from lower semi-continuity, as in [San15, Theorem 1.5]). Thus for  $\pi$ -almost-every  $(x, y)$ ,  $c(x, y) = 0$ , which by assumption gives  $x = y$ , hence (using the same technique as in [San15, Proposition 5.1]) for any test function  $\phi \in \mathcal{C}^0(E, \mathbb{R})$ :

$$\int_E \phi(x) d\mu(x) = \int_{E^2} \phi(x) d\pi(x, y) = \int_{E^2} \phi(y) d\pi(x, y) = \int_E \phi(y) d\nu(y),$$

which shows that  $\mu = \nu$ . □

**Remark 2.4.** *Throughout this work, we work in the compact setting (see Assumption 1), which alleviates substantial technicalities. For the costs  $c(x, y) := \|x - y\|^p$  for some norm  $\|\cdot\|$  on  $\mathbb{R}^d$ , we believe that our results can be shown with careful assumptions on the moments of the measures (and convergence of the sequence of moments in addition to weak convergence).*

## 3 A Fixed-Point Algorithm

### 3.1 Algorithm Definition

In this section, we define a sequence  $(\mu_t) \in \mathcal{P}(\mathcal{X})^{\mathbb{N}}$  that will approach a barycentre of fixed measures  $\nu_k \in \mathcal{P}(\mathcal{Y}_k)$ . We propose a modified version of the iterated scheme from [Álv+16] to solve Eq. (3). To define an iteration mapping, for  $\mu \in \mathcal{P}(\mathcal{X})$ , we consider the set of multi-marginal couplings

$$\Gamma(\mu) := \left\{ \gamma \in \mathcal{P}(\mathcal{X} \times \mathcal{Y}_1 \times \cdots \times \mathcal{Y}_K) : \forall k \in \llbracket 1, K \rrbracket, \gamma_{0,k} \in \Pi_{c_k}^*(\mu, \nu_k) \right\}, \quad (8)$$

where, for all  $k$ ,  $\gamma_{0,k}$  denotes the  $\mathcal{X} \times \mathcal{Y}_k$  marginal of  $\gamma$  and  $\Pi_{c_k}^*(\mu, \nu_k)$  denotes the set of all optimal couplings for the transport problem between  $\mu$  and  $\nu_k$  associated to the cost function  $c_k$ . The existence of such multi-couplings is a consequence of the well-known “gluing lemma” (see [San15, Lemma 5.5]). The following multi-coupling provides an explicit element of  $\Gamma(\mu)$  given  $\pi_k \in \Pi_{c_k}^*(\mu, \nu_k)$ :

$$\gamma(dx, dy_1, \dots, dy_K) := \mu(dx) \pi_1^x(dy_1) \cdots \pi_K^x(dy_K), \quad (9)$$

where we wrote the disintegration of  $\pi_k$  with respect to its first marginal  $\mu$  as  $\pi_k(dx, dy_k) = \mu(dx) \pi_k^x(dy_k)$ . By abuse of notation, we will denote  $B\#\gamma := B\#\gamma_{1,\dots,K}$ , where  $\gamma_{1,\dots,K} \in \mathcal{P}(\mathcal{Y}_1 \times \cdots \times \mathcal{Y}_K)$  is the marginal of  $\gamma$  with respect to  $(y_1, \dots, y_K)$ . In terms of random variables, if  $(X, Y_1, \dots, Y_K) \sim \gamma$ , then  $B\#\gamma = \text{Law}[B(Y_1, \dots, Y_K)]$ . Denoting  $B\#\Gamma(\mu) :=$

$\{B\#\gamma, \gamma \in \Gamma(\mu)\}$ , we define the multi-valued mapping  $G$  which maps  $\mu \in \mathcal{P}(\mathcal{X})$  to the set of next iterates  $G(\mu) \subset \mathcal{P}(\mathcal{X})$ :

$$G := \begin{cases} \mathcal{P}(\mathcal{X}) & \ni & \mathcal{P}(\mathcal{X}) \\ \mu & \mapsto & B\#\Gamma(\mu) \end{cases} . \quad (10)$$

Note that this construction is similar to that of [Álv+16, Remark 3.4]. Moreover, the candidate barycentre  $\bar{\mu} = B\#\gamma_{1,\dots,K}$  is closely related to the multi-marginal formulation of the barycentre problem (see Eq. (7)). Indeed, set  $\pi := \gamma_{1,\dots,K} \in \Pi(\mu_1, \dots, \mu_K)$ , notice that  $\pi$  is a candidate for the multi-marginal problem of a particular structure induced by the reference measure  $\mu$ . In the case where the plans  $\gamma_{0,k}$  are induced by maps  $T_k$ , then this structure is the coupling  $(T_1, \dots, T_K)\#\mu$ . In terms of random variables, if  $X \sim \mu$ , then the chosen coupling is  $(T_1(X), \dots, T_K(X))$ .

Taking inspiration from the  $W_2^2$  case, we can see informally the iterate  $\bar{\mu} \in G(\mu)$  as a local linearisation of  $\mathcal{P}(\mathcal{X})$ . To illustrate this intuition, we consider the case  $\mathcal{X} = \mathcal{Y}_1 = \dots = \mathcal{Y}_K$  and assume that for each  $k$ , the set of optimal plans  $\Pi_{c_k}^*(\mu, \nu_k)$  is reduced to  $(I, T_k)$ , or in other words, that the Monge problem has a unique solution. Informally, one may see the set of maps  $T : \mathcal{X} \rightarrow \mathcal{X}$  sending  $\mu$  to a measure  $T\#\mu \in \mathcal{P}(\mathcal{X})$  as the tangent space to  $\mathcal{P}(\mathcal{X})$  at  $\mu$ . As a result, the problem of finding a barycentre  $\bar{\mu}$  can be seen from the viewpoint of the reference measure  $\mu$  in the tangent space  $T_\mu\mathcal{P}(\mathcal{X})$  as the problem of finding  $S \in T_\mu\mathcal{P}(\mathcal{X})$  such that  $S\#\mu$  would minimise the cost  $V$ . Our approach takes a barycentre of the optimal maps  $T_k$  by choosing the candidate  $S := B \circ (T_1, \dots, T_K)$ . In the case of the squared-Euclidean cost on the common space  $\mathbb{R}^d$ , this amounts to  $S := \sum_k \lambda_k T_k$ , which is exactly the Linearised Optimal Transport barycentre approximation for the reference measure  $\mu$ , as introduced in [MDC20, Section 4.3]. We illustrate this viewpoint schematically in Fig. 1.

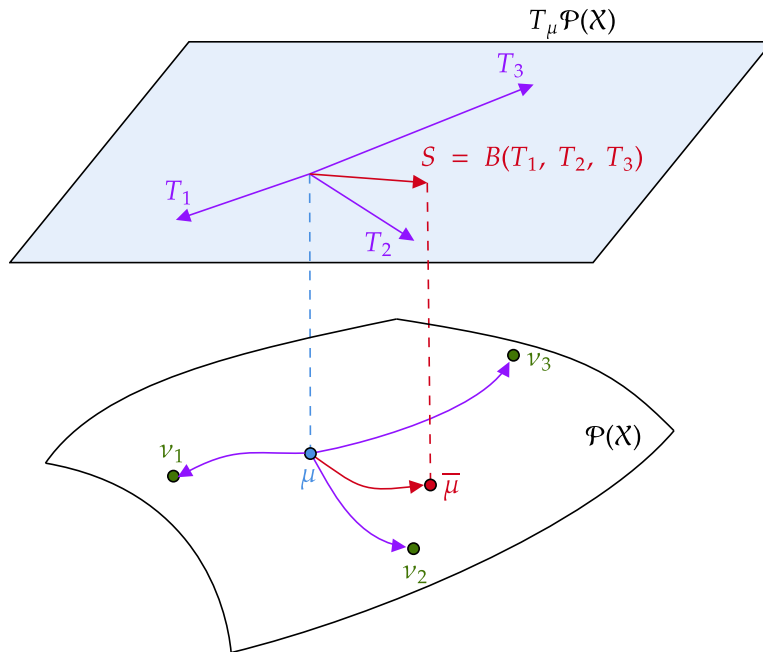


Figure 1: Illustration of the informal linearisation interpretation for the barycentre candidate  $\bar{\mu} = B \circ (T_1, \dots, T_K)\#\mu$ .

Starting from a measure  $\mu_0 \in \mathcal{P}(\mathcal{X})$ , our algorithm consists of choosing iterates through the multi-function  $G$ :

$$\forall t \in \mathbb{N}, \mu_{t+1} \in G(\mu_t).$$

We dedicate the next section to a theoretical study of the convergence of this fixed-point iteration.

### 3.2 Convergence of Fixed-Point Iterations

We can formulate a regularity result of the multi-valued map  $G$ : namely, we will show that  $G$  is *upper hemi-continuous*. For the sake of simplicity, we will take the following definition<sup>2</sup>:

**Definition 3.1.** A multi-valued function  $\varphi : E \rightrightarrows F$  from a compact metric space  $E$  to parts of a compact metric space  $F$  is said to be *upper hemi-continuous (u.h.c.)* if for any sequence  $(x_n, y_n) \in (E \times F)^{\mathbb{N}}$  such that  $y_n \in \varphi(x_n)$  and  $x_n \xrightarrow[n \rightarrow +\infty]{} x \in E$ , there exists an extraction such that  $y_{\alpha(n)} \xrightarrow[n \rightarrow +\infty]{} y \in F$  with  $y \in \varphi(x)$ .

For more technical reasons, we also need to introduce the notion of *lower hemi-continuity*<sup>3</sup>

**Definition 3.2.** A multi-valued function  $\varphi : E \rightrightarrows F$  from a compact metric space  $E$  to parts of a compact metric space  $F$  is said to be *lower hemi-continuous (l.h.c.)* if for any sequence  $(x_n) \in E^{\mathbb{N}}$  such that  $x_n \xrightarrow[n \rightarrow +\infty]{} x \in E$ , then for any  $y \in F$  such that  $y \in \varphi(x)$ , there exists an extraction  $\alpha$  and a sequence  $(y_n) \in F^{\mathbb{N}}$  such that  $y_n \in \varphi(x_{\alpha(n)})$  and  $y_n \xrightarrow[n \rightarrow +\infty]{} y$ .

To illustrate the technical differences between these two notions, we consider two specific multi-valued functions in Fig. 2. Finally, an hemi-continuous multi-map is one that is both u.h.c. and l.h.c.:

**Definition 3.3.** A multi-valued function  $\varphi : E \rightrightarrows F$  from a compact metric space  $E$  to parts of a compact metric space  $F$  is said to be *hemi-continuous* if it is both u.h.c. (Definition 3.1) and l.h.c. (Definition 3.2).

We begin with technical lemmas on the hemi-continuity properties of sets of couplings.

**Lemma 3.4.** Consider  $E, F$  compact metric spaces and  $\nu \in \mathcal{P}(F)$ . The multi-function

$$\Pi_\nu := \begin{cases} \mathcal{P}(E) & \rightrightarrows & \mathcal{P}(E \times F) \\ \mu & \mapsto & \Pi(\mu, \nu) \end{cases} \quad (11)$$

is *hemi-continuous*.

**Proof. u.h.c..** We apply Definition 3.1: introduce  $\mu_n \xrightarrow[n \rightarrow +\infty]{w} \mu \in \mathcal{P}(E)$  and  $\pi_n \in \Pi(\mu_n, \nu)$ . Since  $\mathcal{P}(E \times F)$  is compact, we can introduce  $\alpha$  an extraction such that  $\pi_{\alpha(n)} \xrightarrow[n \rightarrow +\infty]{w} \pi \in \mathcal{P}(E \times F)$ . By continuity of marginalisation, we deduce  $\pi \in \Pi(\mu, \nu)$ , which shows that  $\Pi_\nu$  is u.h.c. by definition.

**l.h.c..** We consider  $W_1$ , the 1-Wasserstein distance on  $\mathcal{P}(E)$  (i.e.  $\mathcal{T}_{d_E}$ ), and use the same

<sup>2</sup>We refer to [AB94, Chapter 17] for a more general definition and introduction to these concepts on Polish spaces. We choose a stronger sequential definition from [AB94, Theorem 17.20], which in their vocabulary corresponds to u.h.c multi-functions with compact values.

<sup>3</sup>whose formulation is equivalent to [AB94, Definition 17.2], by [AB94, Theorem 17.21].

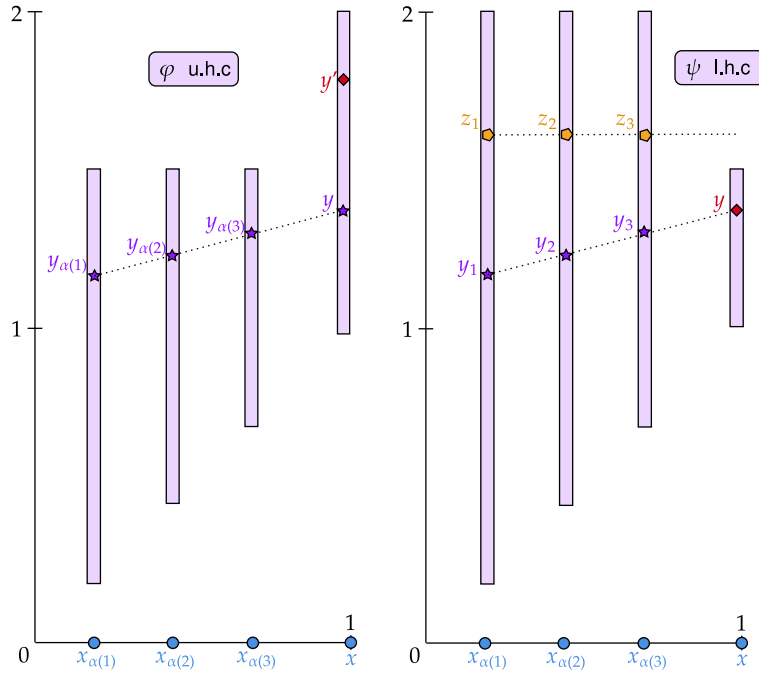


Figure 2: *Left:* the multi-function  $\varphi : [0, 1] \rightrightarrows [0, 2]$  defined by  $\forall x \in [0, 1), \varphi(x) = [x, 3/2]$  and  $\varphi(1) = [1, 2]$  is u.h.c.. Indeed, taking any sequence  $(x_n, y_n)$  such that  $y_n \in \varphi(x_n)$  and  $x_n \xrightarrow[n \rightarrow +\infty]{} x$ , there exists an extraction  $\alpha$  such that  $y_{\alpha(n)} \xrightarrow[n \rightarrow +\infty]{} y \in \varphi(x)$ . However,  $\varphi$  is not l.h.c. at 1 since the target  $y' := 7/4 \in \varphi(1)$  can never be a limit of a sequence  $(x_n, y_n)$  with  $x_n \xrightarrow[n \rightarrow +\infty]{} 1$  and  $y_n \in \varphi(x_n)$ .

*Right:*  $\psi : [0, 1] \rightrightarrows [0, 2]$  defined by  $\forall x \in [0, 1), \psi(x) = [x, 2]$  and  $\psi(1) = [1, 3/2]$  is l.h.c.. Take  $x_n \xrightarrow[n \rightarrow +\infty]{} x$  and a target  $y \in \psi(x)$ . Then there exists an extraction  $\alpha$  and a sequence  $(y_n)$  such that  $y_n \in \psi(x_n)$  and  $y_n \xrightarrow[n \rightarrow +\infty]{} y$ . However,  $\psi$  is not u.h.c: take  $x_n \xrightarrow[n \rightarrow +\infty]{} 1$  and the sequence  $z_n := 5/3$ . We have  $\forall n \in \mathbb{N}, z_n \in \psi(x_n)$ , however any subsequence of  $(z_n)$  converges to  $5/3 \notin \psi(1)$ .

notation for the 1-Wasserstein distance on  $\mathcal{P}(E \times F)$ , with the distance

$$d_{E \times F}((x, y), (x', y')) := \max(d_E(x, x'), d_F(y, y')),$$

both of which metrize the weak convergence by [Vil09, Corollary 6.13]. We apply [Definition 3.2](#): take  $\mu_n \xrightarrow[n \rightarrow +\infty]{w} \mu \in \mathcal{P}(E)$ , and let  $\pi \in \Pi(\mu, \nu)$ . Consider  $(X, Y)$  two coupled random variables of law  $\pi$ , and for  $n \in \mathbb{N}$ , take  $X_n$  a random variable such that  $(X, X_n)$  is an optimal coupling for  $W_1(\mu, \mu_n)$ , and let  $\pi_n := \text{Law}(X_n, Y)$ . We have

$$W_1(\pi, \pi_n) \leq \mathbb{E}[d_{E \times F}((X, Y), (X_n, Y))] = \mathbb{E}[\max(d_E(X, X_n), d_F(Y, Y))] = W_1(\mu, \mu_n),$$

then by metrisation, we get  $W_1(\mu, \mu_n) \xrightarrow[n \rightarrow +\infty]{} 0$ , then  $\pi_n \xrightarrow[n \rightarrow +\infty]{w} \pi$ , concluding the proof that  $\Pi_\nu$  is l.h.c..  $\square$

We can apply Berge's maximisation theorem to show that the set of *optimal* transport plans is upper hemi-continuous for a continuous cost function:

**Lemma 3.5.** Consider  $E, F$  compact metric spaces, a continuous cost  $c : E \times F \rightarrow \mathbb{R}_+$  and  $\nu \in \mathcal{P}(F)$ . The multi-function

$$[\Pi_c^*]_\nu := \begin{cases} \mathcal{P}(E) & \rightrightarrows \mathcal{P}(E \times F) \\ \mu & \mapsto \Pi_c^*(\mu, \nu) \end{cases} \quad (12)$$

is upper hemi-continuous.

**Proof.** By compactness, the map  $\pi \mapsto \int_{E \times F} c d\pi$  is continuous, and by Lemma 3.4, the multi-map  $\mu \rightrightarrows \Pi(\mu, \nu)$  is hemi-continuous (with compact values), hence by Berge's maximisation theorem from [AB94, Theorem 17.31], the map

$$[\Pi_c^*]_\nu : \mu \mapsto \Pi_c^*(\mu, \nu) = \operatorname{argmin}_{\pi \in \Pi(\mu, \nu)} \int_{E \times F} c d\pi$$

is upper hemi-continuous.  $\square$

**Remark 3.6.** Lemma 3.5 can also be deduced from [Vil09, Corollary 5.21].

**Remark 3.7.** The multifunction  $[\Pi_c^*]_\nu$  is not **lower** hemi-continuous. Indeed, take the following points of  $\mathbb{R}^2$ :

$$\forall n \in \mathbb{N}, x_n := (-1, 2^{-n}), y_n := (1, -2^{-n}), x_\infty := (-1, 0), y_\infty := (1, 0), w := (0, 1), z := (0, -1),$$

and the following discrete measures (see Fig. 3):

$$\forall n \in \mathbb{N}, \mu_n := \frac{1}{2}(\delta_{x_n} + \delta_{y_n}), \mu_\infty := \frac{1}{2}(\delta_{x_\infty} + \delta_{y_\infty}), \nu := \frac{1}{2}(\delta_w + \delta_z).$$

We have  $\mu_n \xrightarrow[n \rightarrow +\infty]{w} \mu_\infty$ , and a unique OT plan for the cost  $c(\cdot, \cdot) := \|\cdot - \cdot\|_2^2$  between  $\mu_n$  and  $\nu$ , which sends  $x_n$  to  $w$  and  $y_n$  to  $z$ :

$$\forall n \in \mathbb{N}, \Pi_c^*(\mu_n, \nu) = \{\pi_n\}, \pi_n := \frac{1}{2}(\delta_{x_n, w} + \delta_{y_n, z}),$$

with  $\pi_n \xrightarrow[n \rightarrow +\infty]{w} \pi_\infty := \frac{1}{2}(\delta_{x_\infty, w} + \delta_{y_\infty, z})$ . However, the set of optimal plans between the limit  $\mu_\infty$  and  $\nu$  has more than one element, since  $\|x_\infty - w\|_2^2 = \|x_\infty - z\|_2^2$  and  $\|y_\infty - w\|_2^2 = \|y_\infty - z\|_2^2$ :

$$\Pi_c^*(\mu, \nu) = \{(1-t)\pi_\infty + t\pi', t \in [0, 1]\}, \pi' := \frac{1}{2}(\delta_{x_\infty, z} + \delta_{y_\infty, w}).$$

We conclude that there does not exist an extraction  $\alpha$  and a sequence  $(\pi'_n)$  such that  $\forall n \in \mathbb{N}, \pi'_n \in \Pi_c^*(\mu_{\alpha(n)}, \nu)$  and  $\pi'_n \xrightarrow[n \rightarrow +\infty]{w} \pi'$ .

A direct corollary of Lemma 3.5 is the upper hemi-continuity of  $\Gamma$  and  $G$ . For notational convenience, we introduce  $\mathcal{Z} := \mathcal{X} \times \mathcal{Y}_1 \times \cdots \times \mathcal{Y}_K$ .

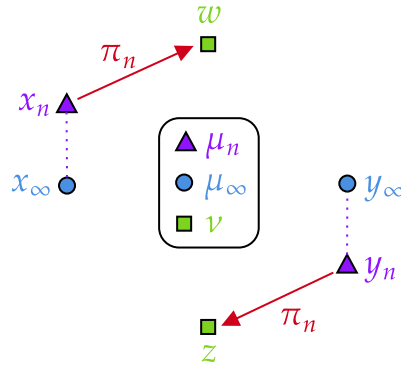


Figure 3: Counter-example from Remark 3.7 showing that  $\Pi_c^*(\cdot, \nu)$  is not lower hemi-continuous in general.

**Proposition 3.8.** *The multi-map*

$$\Gamma := \begin{cases} \mathcal{P}(\mathcal{X}) & \rightrightarrows \mathcal{P}(\mathcal{Z}) \\ \mu & \mapsto \Gamma(\mu) \end{cases}$$

where  $\Gamma(\mu)$  is defined in Eq. (8) and  $G$  defined in Eq. (10) are upper hemi-continuous (and compact-valued).

**Proof.** Let  $\mu \in \mathcal{P}(\mathcal{X})$ . To show that  $G(\mu)$  and  $\Gamma(\mu)$  are compact, it suffices to show that  $\Gamma(\mu)$  is closed, since  $\mathcal{P}(\mathcal{Z})$  is compact, and  $G(\mu) = B\#\Gamma(\mu)$  with  $B$  continuous by Lemma 2.2. Take  $(\gamma_n) \in \Gamma(\mu)^\mathbb{N}$  such that  $\gamma_n \xrightarrow{n \rightarrow +\infty} \gamma \in \mathcal{P}(\mathcal{Z})$ . We show that  $\gamma \in \Gamma(\mu)$ . For  $k \in \llbracket 1, K \rrbracket$  and  $n \in \mathbb{N}$ , we have  $\gamma_n \in \Gamma(\mu)$ , hence  $[\gamma_n]_{0,k} \in \Pi_{c_k}^*(\mu, \nu_k)$ . By continuity of marginalisation, we deduce that  $\gamma \in \Pi(\mu, \nu_1, \dots, \nu_K)$ . By continuity of  $\pi \mapsto \int_{\mathcal{X} \times \mathcal{Y}_k} c_k d\pi$  (which holds by compactness), we deduce that  $\gamma_{0,k} \in \Pi_{c_k}^*(\mu, \nu_k)$ , hence  $\gamma \in \Gamma(\mu)$ . For the u.h.c. of  $\Gamma$ , take a sequence  $(\mu_n) \in \mathcal{P}(\mathcal{X})^\mathbb{N}$  such that  $\mu_n \xrightarrow{n \rightarrow +\infty} \mu \in \mathcal{P}(\mathcal{X})$ , and take a sequence  $(\gamma_n) \in \mathcal{P}(\mathcal{Z})^\mathbb{N}$ , with  $\gamma_n \in \Gamma(\mu_n)$ . Since  $\gamma_n \in \mathcal{P}(\mathcal{Z})$  which is compact, take  $\alpha$  an extraction such that  $\gamma_{\alpha(n)} \xrightarrow{n \rightarrow +\infty} \gamma \in \mathcal{P}(\mathcal{Z})$ . We will show that  $\gamma \in \Gamma(\mu)$ .

Start with  $k := 1$ . For  $n \in \mathbb{N}$ , we have  $\gamma_{\alpha(n)} \in \Gamma(\mu_{\alpha(n)})$ , hence  $\pi_{\alpha(n)}^{(1)} := [\gamma_{\alpha(n)}]_{0,1} \in \Pi_{c_1}^*(\mu_{\alpha(n)}, \nu_1)$ . By Lemma 3.5, the map  $\mu \mapsto \Pi_{c_1}^*(\mu, \nu_1)$  is u.h.c., hence by definition, since  $\mu_{\alpha(n)} \xrightarrow{n \rightarrow +\infty} \mu \in \mathcal{P}(\mathcal{X})$  and  $\pi_{\alpha(n)}^{(1)} \in \Pi_{c_1}^*(\mu_{\alpha(n)}, \nu_1)$ , there exists an extraction  $\alpha_1$  such that  $\pi_{\alpha \circ \alpha_1(n)}^{(1)} \xrightarrow{n \rightarrow +\infty} \pi^{(1)} \in \Pi_{c_1}^*(\mu, \nu_1)$ .

Continuing this method for  $k \in \llbracket 2, K \rrbracket$  with successive sub-extractions  $\alpha_k$ , setting  $\beta := \alpha \circ \alpha_1 \circ \dots \circ \alpha_K$ , we have for any  $k \in \llbracket 1, K \rrbracket$ ,  $[\gamma_{\beta(n)}]_{0,k} = \pi_{\beta(n)}^{(k)} \xrightarrow{n \rightarrow +\infty} \pi^{(k)} \in \Pi_{c_k}^*(\mu, \nu_k)$ .

The continuity of marginalisation implies  $\gamma_{0,k} = \pi^{(k)}$ , and in turn shows that  $\gamma \in \Gamma(\mu)$ , concluding that  $\Gamma$  is u.h.c.

For  $G$ , the fact that  $G(\mu) = B\#\Gamma(\mu)$  and the continuity of  $B$  prove that  $G$  is u.h.c. using the u.h.c. of  $\Gamma$  by [AB94, Theorem 17.23].  $\square$

In order to study the energy of iterates of  $G$ , we first require a technical result on the error of sub-optimal ground barycentres for  $B$ . We introduce a radius constant  $R := \max_{(x,Y) \in \mathcal{X} \times \mathcal{Y}} d_{\mathcal{X}}(x, B(Y))$ . Note that  $R > 0$ . Indeed, let  $a, b \in \mathcal{X}$  be such that  $d_{\mathcal{X}}(a, b) = \text{diam}(\mathcal{X})$ . Then, for all  $Y \in \mathcal{Y}$ ,

it holds

$$2R \geq d_{\mathcal{X}}(a, B(Y)) + d_{\mathcal{X}}(B(Y), b) \geq d_{\mathcal{X}}(a, b) = \text{diam}(\mathcal{X}),$$

and so  $R \geq \text{diam}(\mathcal{X})/2 > 0$ .

**Lemma 3.9.** *There exists a function  $\delta = \eta \circ d_{\mathcal{X}}$ , with  $\eta : [0, R] \rightarrow \mathbb{R}_+$  lower-semi-continuous, non-decreasing and verifying  $\eta(s) = 0 \iff s = 0$ , such that*

$$\forall (x, Y) \in \mathcal{X} \times \mathcal{Y}, C(x, Y) \geq C(B(Y), Y) + \delta(x, B(Y)). \quad (13)$$

**Proof.** — *Step 1:* Definition of  $\eta$ . First, for  $(x, Y) \in \mathcal{X} \times \mathcal{Y}$ , let  $\Delta(x, Y) := C(x, Y) - C(B(Y), Y)$ . By definition of  $B$ ,  $\Delta(x, Y) \geq 0$ , and  $\Delta(x, Y) = 0 \iff x = B(Y)$ . By assumption,  $B$  and  $C$  are continuous, which implies that  $\Delta$  is also continuous.

We now introduce  $S := \max_{(x, Y) \in \mathcal{X} \times \mathcal{Y}} \Delta(x, Y)$ .  $R > 0$  ensures  $S > 0$ . Define now the function  $\eta$ :

$$\eta := \begin{cases} [0, R] & \longrightarrow & [0, S] \\ u & \longmapsto & \min_{(x, Y) \in \mathcal{X} \times \mathcal{Y}} \{ \Delta(x, Y) : d_{\mathcal{X}}(x, B(Y)) \geq u \} \end{cases} \cdot \quad (14)$$

We show that for  $u \in [0, R]$ , the infimum is attained. First, let  $f := (x, Y) \mapsto d_{\mathcal{X}}(x, B(Y))$ , we remark that

$$\forall (x, Y) \in \mathcal{X} \times \mathcal{Y}, d_{\mathcal{X}}(x, B(Y)) \geq u \iff (x, Y) \in f^{-1}([u, R]).$$

By continuity of  $f$  and compactness of  $\mathcal{X} \times \mathcal{Y}$ ,  $\mathcal{K}_u := f^{-1}([u, R])$  is a compact subset of  $\mathcal{X} \times \mathcal{Y}$ .  $\mathcal{K}_u$  is not empty since there exists  $(x_R, Y_R) \in \mathcal{X} \times \mathcal{Y}$  such that  $d_{\mathcal{X}}(x_R, B(Y_R)) = R$  (by continuity, compactness and definition of  $R$ ).

— *Step 2:* Proof of Eq. (13). Let  $(x, Y) \in \mathcal{X} \times \mathcal{Y}$ , and  $u := d_{\mathcal{X}}(x, B(Y))$ . By definition,  $(x, Y) \in \mathcal{K}_u$ , hence  $\eta(u) \leq \Delta(x, Y)$ , which is equivalent to Eq. (13).

— *Step 3:* Lower semi-continuity of  $\eta$ . Let  $u_n \xrightarrow{n \rightarrow +\infty} u \in [0, R]$ , and for  $n \in \mathbb{N}$  introduce  $(x_n, Y_n) \in \mathcal{K}_{u_n}$  such that  $\eta(u_n) = \Delta(x_n, Y_n)$ . Since  $(\eta(u_n)) \in [0, S]^{\mathbb{N}}$ , consider an extraction  $\alpha$  such that  $\eta(u_{\alpha(n)}) \xrightarrow{n \rightarrow +\infty} a_{\alpha} \in [0, S]$ . By compactness of  $\mathcal{X} \times \mathcal{Y}$ , we can extract from  $(x_{\alpha(n)}, Y_{\alpha(n)})_n$  a subsequence such that  $(x_{\alpha \circ \beta(n)}, Y_{\alpha \circ \beta(n)}) \xrightarrow{n \rightarrow +\infty} (x_{\alpha, \beta}, Y_{\alpha, \beta}) \in \mathcal{X} \times \mathcal{Y}$ . By construction of the sequence  $(x_n, Y_n)_n$ , we have

$$\forall n \in \mathbb{N}, d_{\mathcal{X}}(x_{\alpha \circ \beta(n)}, B(Y_{\alpha \circ \beta(n)})) \geq u_{\alpha \circ \beta(n)}, \quad (15)$$

since  $(x_{\alpha \circ \beta(n)}, Y_{\alpha \circ \beta(n)}) \in \mathcal{K}_{u_{\alpha \circ \beta(n)}}$ . Taking the limit in Eq. (15) yields  $d_{\mathcal{X}}(x_{\alpha, \beta}, B(Y_{\alpha, \beta})) \geq u$ , by continuity of  $B$ , Lemma 2.2. This shows that  $(x_{\alpha, \beta}, Y_{\alpha, \beta}) \in \mathcal{K}_u$ , hence  $\eta(u) \leq \Delta(x_{\alpha, \beta}, Y_{\alpha, \beta})$ . However, by continuity of  $\Delta$ , and since  $\Delta(x_{\alpha(n)}, Y_{\alpha(n)}) \xrightarrow{n \rightarrow +\infty} a_{\alpha}$ , it follows that  $\Delta(x_{\alpha, \beta}, Y_{\alpha, \beta}) = a_{\alpha}$ . Since the subsequential limit  $a_{\alpha}$  was chosen arbitrarily, we conclude that  $\eta(u) \leq \liminf_{n \rightarrow +\infty} \eta(u_n)$ , hence  $\eta$  is lower semi-continuous.

— *Step 4:*  $\eta$  is non-decreasing. Let  $0 \leq u \leq v \leq R$ , we have  $\mathcal{K}_v \subset \mathcal{K}_u$ , hence

$$\eta(u) = \min_{(x, Y) \in \mathcal{K}_u} \Delta(x, Y) \leq \min_{(x, Y) \in \mathcal{K}_v} \Delta(x, Y) = \eta(v).$$

— *Step 5:* Separation property. Let  $u \in [0, R]$  such that  $\eta(u) = 0$ . This implies that there exists  $(x, Y) \in \mathcal{X} \times \mathcal{Y}$  such that  $\Delta(x, Y) = 0$  and  $d_{\mathcal{X}}(x, B(Y)) \geq u$ . Now by Step 1 this implies  $x = B(Y)$ , thus  $d_{\mathcal{X}}(x, B(Y)) = 0$  and finally  $u = 0$ .  $\square$

[Lemma 3.9](#) is a generalisation of the following elementary Euclidean property in  $\mathbb{R}^d$  for the cost  $\|\cdot - \cdot\|_2^2$ , for which  $B(y_1, \dots, y_K) = \sum_{k=1}^K \lambda_k y_k$  verifies the following identity:

$$\forall x \in \mathbb{R}^d, \forall (y_1, \dots, y_K) \in (\mathbb{R}^d)^K, \bar{x} := \sum_{k=1}^K \lambda_k y_k : \sum_{k=1}^K \lambda_k \|x - y_k\|_2^2 = \sum_{k=1}^K \lambda_k \|\bar{x} - y_k\|_2^2 + \|x - \bar{x}\|_2^2.$$

Given the inequality in [Eq. \(13\)](#), we can now find an informative inequality between  $V(\bar{\mu})$  and  $V(\mu)$  for any  $\bar{\mu} \in G(\mu)$ .

**Proposition 3.10.** *Let  $\mu \in \mathcal{P}(\mathcal{X})$  and  $\bar{\mu} \in G(\mu)$ . Then  $V(\mu) \geq V(\bar{\mu}) + \mathcal{T}_\delta(\mu, \bar{\mu})$ . If  $\mu^*$  is a barycentre, then  $G(\mu^*) = \{\mu^*\}$ .*

**Proof.** Let  $\bar{\mu} = B\#\gamma \in G(\mu)$  with  $\gamma \in \Gamma(\mu)$ . By definition of  $\mathcal{T}_{c_k}$  and by optimality of the bi-marginals  $\gamma_{0,k}$  of  $\gamma$ :

$$\sum_{k=1}^K \mathcal{T}_{c_k}(\mu, \nu_k) = \int_{\mathcal{X} \times \mathcal{Y}} C(x, Y) d\gamma(x, Y) \quad (16)$$

$$\geq \int_{\mathcal{X} \times \mathcal{Y}} (C(B(Y), Y) + \delta(x, B(Y))) d\gamma(x, Y) \quad (17)$$

$$\geq \sum_{k=1}^K \mathcal{T}_{c_k}(B\#\gamma, \nu_k) + \mathcal{T}_\delta(\mu, B\#\gamma) \quad (18)$$

$$= V(\bar{\mu}) + \mathcal{T}_\delta(\mu, \bar{\mu}). \quad (19)$$

The inequality in [Eq. \(17\)](#) comes from [Lemma 3.9](#), and the inequality in [Eq. \(18\)](#) comes from the definition of  $\Gamma(\mu)$  ([Eq. \(8\)](#)), which allows us to write for  $k \in \llbracket 1, K \rrbracket$ :

$$\int_{\mathcal{X} \times \mathcal{Y}} c_k(B(Y), y_k) d\gamma(x, Y) = \int_{\mathcal{X} \times \mathcal{Y}_k} c_k d\pi_k,$$

where we introduce the coupling  $\pi_k := (B, P_k)\#\gamma_{1, \dots, K}$ , with  $P_k(y_1, \dots, y_K) = y_k$ . The first marginal of  $\pi$  is  $B\#\gamma_{1, \dots, K}$  (which we write  $B\#\gamma$  for legibility), and the second marginal is  $\nu_k$ . Similarly,

$$\int_{\mathcal{X} \times \mathcal{Y}} \delta(x, B(Y)) d\gamma(x, Y) = \int_{\mathcal{X} \times \mathcal{X}} \delta d[(I, B)\#\gamma] \geq \mathcal{T}_\delta(\mu, B\#\gamma).$$

If  $\mu^*$  is a barycentre, then by definition for any  $\bar{\mu} \in G(\mu)$ , we have  $V(\bar{\mu}) \geq V(\mu^*)$ , thus [Eqs. \(17\)](#) and [\(18\)](#) are equalities, and  $\mathcal{T}_\delta(\mu^*, \bar{\mu}) = 0$ . By [Lemmas 2.3](#) and [3.9](#), the cost  $\delta$  guarantees the separation property of the transport cost  $\mathcal{T}_\delta$ , hence  $\mu^* = \bar{\mu}$ .  $\square$

Applying [Proposition 3.10](#) to the  $W_2$  case for absolutely continuous measures yields [[Álv+16](#), [Proposition 4.3](#)], wherein the cost  $\mathcal{T}_\delta$  is simply  $W_2^2$ . This decrease was also studied by [[Lin23](#), [Proposition 4.4](#)] in the discrete setting  $W_p^p$ .

The inequality in [Proposition 3.10](#) shows that the amount of decrease in the energy between two iterations is lower-bounded by a transport discrepancy  $\mathcal{T}_\delta$  (we remind that in the squared-Euclidean case,  $\mathcal{T}_\delta = W_2^2$ ). We can now show convergence of iterates of  $G$ , in the sense that any weakly converging subsequence converges towards a fixed point of  $G$ .

**Theorem 3.11.** *For any  $\mu_0 \in \mathcal{P}(\mathcal{X})$ , let  $(\mu_t)$  verifying  $\mu_{t+1} \in G(\mu_t)$ . Then  $(\mu_t)$  has converging subsequences, and any weakly converging subsequence necessarily converges towards a  $\mu \in \mathcal{P}(\mathcal{X})$  such that  $\mu \in G(\mu)$ .*

**Proof.** Fix a sequence  $(\mu_t)$  such that  $\mu_{t+1} \in G(\mu_t)$  and write  $\mu_{t+1} = B\#[\gamma_t]_{1,\dots,K}$  with  $\gamma_t \in \Gamma(\mu_t)$ . Since  $\mathcal{X}$  is compact, the space  $\mathcal{P}(\mathcal{X})$  is also compact, and so the sequence  $(\mu_t)$  is tight. Consider an extraction  $\alpha$  such that  $\mu_{\alpha(t)} \xrightarrow[t \rightarrow +\infty]{w} \mu \in \mathcal{P}(\mathcal{X})$ . By u.h.c. of  $\Gamma$  (Proposition 3.8), there exists an extraction  $\beta$  such that  $\gamma_{\alpha\beta(t)} \xrightarrow[t \rightarrow +\infty]{w} \gamma \in \Gamma(\mu)$ .

By Proposition 3.10, the sequence  $(V(\mu_t))$  is non-increasing and non-negative, hence it is convergent, and as a result,  $\lim_{t \rightarrow +\infty} [V(\mu_{\alpha\beta(t)}) - V(\mu_{\alpha\beta(t)+1})] = 0$ . Using the lower-bound in Proposition 3.10 we obtain:

$$\forall t \in \mathbb{N}, 0 \leq \mathcal{T}_\delta(\mu_{\alpha\beta(t)}, \mu_{\alpha\beta(t)+1}) \leq V(\mu_{\alpha\beta(t)}) - V(\mu_{\alpha\beta(t)+1}),$$

and take the limit inferior:

$$0 \leq \liminf_{t \rightarrow +\infty} \mathcal{T}_\delta(\mu_{\alpha\beta(t)}, \mu_{\alpha\beta(t)+1}) \leq 0. \quad (20)$$

We remind that  $(\mu_{\alpha\beta(t)+1})_t$  is a sequence in  $\mathcal{P}(\mathcal{X})$  which is compact, and take  $\rho \in \mathcal{P}(\mathcal{X})$  a subsequential limit of  $(\mu_{\alpha\beta(t)+1})_t$ . By lower-semi-continuity of  $\mathcal{T}_\delta$  (which holds by applying Lemma 2.3 item 1) with Lemma 3.9), Eq. (20) provides  $\mathcal{T}_\delta(\mu, \rho) = 0$ . By Lemma 2.3 item 3), we obtain that  $\rho = \mu$ , thus any subsequential limit of  $(\mu_{\alpha\beta(t)+1})_t$  is  $\mu$ , which proves that it converges weakly to  $\mu$ .

Writing abusively  $B\#\gamma$  for  $B\#\gamma_{1,\dots,K}$ , we conclude:

$$\begin{array}{ccc} \mu_{\alpha\beta(t)+1} & \xrightarrow[t \rightarrow +\infty]{w} & \mu \\ \parallel & & \parallel \\ B\#\gamma_{\alpha\beta(t)} & \xrightarrow[t \rightarrow +\infty]{w} & B\#\gamma \end{array}$$

hence we have found  $\gamma \in \Gamma(\mu)$  such that  $\mu = B\#\gamma$ , proving  $\mu \in G(\mu)$ .  $\square$

**Remark 3.12.** *Fixed-points of  $G$  may not be unique and may not be barycentres, as shown the the following example. Take the following measures:*

$$\mu := \frac{1}{2} (\delta_{(0,1)} + \delta_{(0,-1)}), \quad \nu_1 := \frac{1}{2} (\delta_{(-2,1)} + \delta_{(2,-1)}), \quad \nu_2 := \frac{1}{2} (\delta_{(-2,-1)} + \delta_{(2,1)}).$$

Between  $\mu$  and  $\nu_k$ , the unique OT plan for the squared-Euclidean cost is given by a permutation, with

$$\pi_1^* = \frac{1}{2} (\delta_{(0,1) \otimes (-2,1)} + \delta_{(0,-1) \otimes (2,-1)}),$$

and likewise for  $\pi_2^*$ . The next iterate of  $G$  and  $H$  are both equal to  $\mu$  itself, which is distinct from the unique barycenter  $\mu^* = \frac{1}{2} (\delta_{(-2,0)} + \delta_{(2,0)})$ . We show this example in Fig. 4.

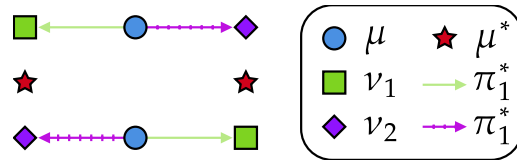


Figure 4: Example showing a non-barycentre measure  $\mu$  which is a fixed-point of  $G$  and  $H$ .

### 3.3 Expression of the Iterates when the Plans are Maps

In some cases, the plans introduced in  $\Gamma(\mu)$  (Eq. (8)) are induced by maps, which is to say that they are each supported on a set of the form  $(x, T_k(x))$ . This is the case in the specific setting chosen by [Álv+16], which is to say that all measures are absolutely continuous on  $\mathbb{R}^d$  and the costs are all  $c(x, y) = \|x - y\|_2^2$ . By Brenier's Theorem (as stated in [San15, Theorem 1.22], for example), this implies that optimal transport couplings are supported on the graph of a map. This property holds under the weaker condition that the costs verify the Twist condition (see [Vil09, Theorem 10.28] for example). In this case, each set optimal transport plans  $\Pi_{c_k}^*(\mu, \nu_k)$  is composed of one element  $(I, T_k)\#\mu$ , and as a result, the expression of  $G(\mu)$  becomes substantially simpler, namely  $G(\mu) = \{B \circ (T_1, \dots, T_K)\#\mu\}$ . In the linearisation interpretation (Fig. 1), this expression can be understood as taking the ground barycentre of the maps  $T_k$  using the ground map  $B$ .

Drawing inspiration from this observation, we can define an alternative iteration consisting in choosing a map  $T_k$  as the barycentric projection of the coupling  $\gamma_{0,k} \in \Pi_{c_k}^*(\mu, \nu_k)$  for  $\gamma \in \Gamma(\mu)$ : see Definition 3.13 and Fig. 5.

**Definition 3.13.** *The **barycentric projection** of a coupling  $\pi \in \Pi(\mu, \nu)$  for  $\mu \in \mathcal{P}(E)$  and  $\nu \in \mathcal{P}(F)$  is the map  $\bar{\pi} : E \rightarrow F$ , which is defined for  $\mu$ -almost-every  $x \in E$  as:*

$$\bar{\pi}(x) = \int_F y \pi^x(dy),$$

where we wrote the disintegration  $\pi(dx, dy) = \mu(dx) \pi^x(dy)$ . In terms of random variables, one may write this expression as:

$$\bar{\pi}(x) = \mathbb{E}_{(X,Y) \sim \pi} [Y \mid X = x].$$

Note that for this expression to be well-defined, the target space  $F$  must be a *convex space*, i.e. a space where one may define convex combinations of points (or, more precisely, expectations of probability measures). In the case  $\mathcal{X} = \mathcal{Y}_1 = \dots = \mathcal{Y}_K$ , a meaningful choice of convex combination is the ground barycentre  $B$ . We can apply this barycentric projection idea to define an alternate multi-mapping  $H : \mathcal{P}(\mathcal{X}) \rightrightarrows \mathcal{P}(\mathcal{X})$ :

$$\forall \mu \in \mathcal{P}(\mathcal{X}), H(\mu) := \{B \circ (\overline{\gamma_{0,1}}, \dots, \overline{\gamma_{0,K}})\#\mu, \gamma \in \Gamma(\mu)\}. \quad (21)$$

In general, for  $\pi \in \Pi(\mu, \nu)$ ,  $\bar{\pi}\#\mu \neq \nu$ , hence one does not necessarily have  $\forall \tilde{\mu} \in H(\mu), V(\tilde{\mu}) \leq V(\mu)$ . However, if each  $\Pi_{c_k}^*(\mu, \nu_k)$  are composed of plans supported by maps, then  $H(\mu) = G(\mu)$ . In the case of discrete measures and for the squared Euclidean cost, the iterations of  $H$  correspond to the approach proposed in [CD14, Algorithm 2].

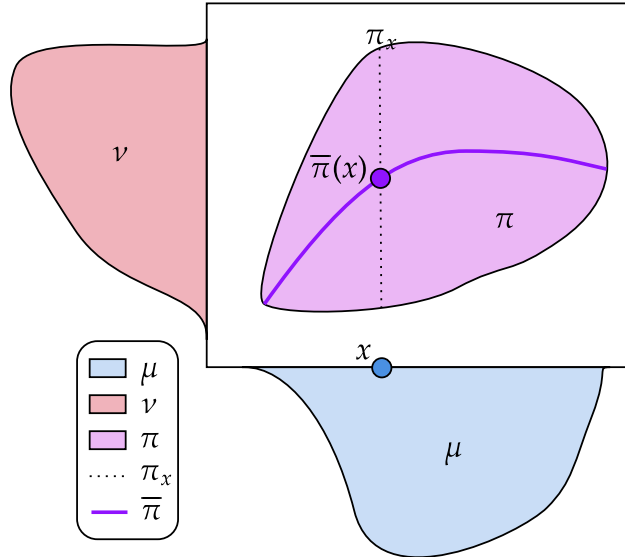


Figure 5: Illustration of a barycentric projection. The disintegration of the coupling  $\pi$  with respect to its first marginal  $\mu$  at  $x$  is the measure  $\pi_x$  concentrated on the dotted line. The barycentric projection of  $\pi$  evaluated at  $x$  is the mean of the measure  $\pi_x$ .

### 3.4 The Particular Case of Conditionally Independent Couplings

In Eq. (8), we chose all possible multi-couplings with optimal bi-marginals. It is possible to restrict the set of couplings to the smaller set of multi-couplings with conditionally independent marginals, i.e. multi-couplings  $\gamma \in \Pi(\mu, \nu_1, \dots, \nu_K)$  such that there exists  $\pi_k \in \Pi_{c_k}^*(\mu, \nu_k)$  for  $k \in \llbracket 1, K \rrbracket$  such that  $\gamma_{0,k} = \pi_k$  and specifically:

$$\gamma(dx, dy_1, \dots, dy_K) := \mu(dx) \pi_1^x(dy_1) \cdots \pi_K^x(dy_K),$$

as in Eq. (9). In terms of random variables, this corresponds to the choice of  $(X, Y_1, \dots, Y_K)$  such that  $(X, Y_k) \sim \pi_k$  and conditionally to  $X$ , the variables  $Y_1, \dots, Y_K$  are independent. We denote by  $\Gamma_{\otimes}(\mu)$  the set of such couplings, and consider the associated multi-map  $G_{\otimes} := B\#\Gamma_{\otimes}$  as in Eq. (10). It is clear that  $\forall \mu \in \mathcal{P}(\mathcal{X})$ ,  $G_{\otimes}(\mu) \subset G(\mu)$ . In particular, this implies subsequential convergence converges of iterates  $\mu_{t+1} = G_{\otimes}(\mu_t)$  to a fixed-point of  $G$ . In Proposition 3.14, we show that the convergence is to a fixed-point of  $G_{\otimes}$  in the discrete case (measures with finite support). First, we emphasise that with a discrete initialisation measure and discrete measures  $(\nu_k)$ , the support of the sequence  $(\mu_t)$  is finite and always contained in:

$$\{B(y_1, \dots, y_K), \forall k \in \llbracket 1, K \rrbracket, y_k \in \text{supp}(\nu_k)\},$$

which ensures that iterates remain discrete.

**Proposition 3.14.** *Take  $\mu_0 \in \mathcal{P}(\mathcal{X})$  a discrete measure and  $\nu_1, \dots, \nu_k \in \mathcal{P}(\mathcal{Y}_1) \times \dots \times \mathcal{P}(\mathcal{Y}_K)$  discrete measures. Then any sub-sequential limit  $\mu \in \mathcal{P}(\mathcal{X})$  of the sequence  $(\mu_t)$  defined by  $\mu_{t+1} \in G_{\otimes}(\mu_t)$  verifies  $\mu \in G_{\otimes}(\mu)$ .*

**Proof.** We follow a technique used in the proof of [Goz+17, Theorem 9.6], specifically page 65. As commented before the statement of the result, the sequence  $(\mu_t)$  remains discrete. Write for  $t \in \mathbb{N}$ ,  $\mu_{t+1} = B\#\gamma_t$  with  $\gamma_t \in \Gamma_{\otimes}(\mu_t)$ , and take an extraction  $\alpha$  such that  $\mu_{\alpha(t)} \xrightarrow[t \rightarrow +\infty]{w} \mu$ . As done in Theorem 3.11, the u.h.c. property of  $\Gamma$  allows us to

extract a subsequence  $\beta$  such that  $\gamma_{\alpha\circ\beta(t)} \xrightarrow[t \rightarrow +\infty]{w} \gamma \in \Gamma(\mu)$ , since we have the (point-wise) inclusion  $\Gamma_{\otimes} \subset \Gamma$ . As shown in the proof of [Theorem 3.11](#), the sequence  $(\mu_{\alpha\circ\beta(t)})_t$  weakly converges to  $\mu$ , hence we now want to show that  $\gamma \in \Gamma_{\otimes}(\mu)$ , which would allow to conclude  $\mu \in G_{\otimes}(\mu)$ .

For  $t \in \mathbb{N}$  and  $k \in \llbracket 1, K \rrbracket$ , introduce  $\pi_{\alpha\circ\beta(t)}^{(k)} := [\gamma_{\alpha\circ\beta(t)}]_{0,k}$ , and its disintegration with respect to  $\mu_{\alpha\circ\beta(t)}$  as

$$\pi_{\alpha\circ\beta(t)}^{(k)}(dx, dy_k) = \mu_{\alpha\circ\beta(t)}(dx) [\pi_{\alpha\circ\beta(t)}^{(k)}]^x(dy_k).$$

As argued above the statement of the proposition, the sequence  $(\mu_t)_t$  remains discrete with a support contained in  $B(\prod_k \text{supp}(\nu_k))$  and thus  $(\gamma_t)$  also remains discrete, and its first marginal  $\mu_t$  has a finite support of size at most  $n := \prod_k \# \text{supp}(\nu_k)$  on fixed points  $(x_1, \dots, x_n)$ . For simplicity, we will see the measures  $(\mu_t)$  as supported on  $\mathcal{X}_n := \{x_1, \dots, x_n\}$  with possibly zero mass at some of these points, and in such cases, we define  $[\pi_{\alpha\circ\beta(t)}^{(k)}]^x$  as the null measure  $\mathcal{M}_0$ . Since  $\gamma_{\alpha\circ\beta(t)} \in \Gamma_{\otimes}(\mu_{\alpha\circ\beta(t)})$ , by definition we can write its disintegration with respect to  $\mu_{\alpha\circ\beta(t)}$  as:

$$\gamma_{\alpha\circ\beta(t)}(dx, dy_1, \dots, dy_K) = \mu_{\alpha\circ\beta(t)}(dx) [\pi_{\alpha\circ\beta(t)}^{(1)}]^x(dy_1) \cdots [\pi_{\alpha\circ\beta(t)}^{(K)}]^x(dy_K).$$

For  $i \in \llbracket 1, n \rrbracket$  and  $k \in \llbracket 1, K \rrbracket$ , there exists an extraction  $\chi_{i,k}$  such that the sequence  $\left([\pi_{\alpha\circ\beta\circ\chi_{i,k}(t)}^{(k)}]^{x_i}\right)_{t \in \mathbb{N}}$  converges weakly to a  $[\pi^{(k)}]^{x_i} \in \mathcal{P}(\mathcal{X}) \times \{\mathcal{M}_0\}$ . We choose the extractions as successive sub-extractions, such that  $\chi_{1,2}$  is a sub-extraction of  $\chi_{1,1}$ , until  $\chi_{n,K}$  which is a sub-extraction of all previous extractions. We then define  $\chi := \chi_{n,K}$ . The extraction  $\chi$  is such that for  $i \in \llbracket 1, n \rrbracket$  and  $k \in \llbracket 1, K \rrbracket$ , the sequence  $\left([\pi_{\alpha\circ\beta\circ\chi(t)}^{(k)}]^{x_i}\right)_{t \in \mathbb{N}}$  converges weakly to  $[\pi^{(k)}]^{x_i}$ . By verifying against test functions, we deduce the following disintegration holds for  $\gamma$ :

$$\gamma(dx, dy_1, \dots, dy_K) = \mu(dx) [\pi^{(1)}]^x(dy_1) \cdots [\pi^{(K)}]^x(dy_K),$$

which shows that  $\gamma \in \Gamma_{\otimes}(\mu)$ , and thus  $\mu \in G_{\otimes}(\mu)$ . □

**Remark 3.15.** *The proof of [Proposition 3.14](#) can also be written for discrete measures with at-most-countable supports through a diagonal extraction argument, we kept to finite supports for legibility.*

## 4 Focus on the Discrete Case

In this section, we will formulate the fixed-point algorithm in the discrete case, and discuss some algorithmic aspects.

### 4.1 Discrete Expression and Algorithms

Consider discrete measures  $\nu_k := \sum_{i=1}^{n_k} b_{k,i} \delta_{y_{k,i}} \in \mathcal{P}(\mathbb{R}^{d_k})$  where  $\forall k \in \llbracket 1, K \rrbracket$ ,  $\forall i \in \llbracket 1, n_k \rrbracket$ ,  $y_{k,i} \in \mathbb{R}^{d_k}$ . We stack the support of  $\nu_k$  into  $Y_k \in \mathbb{R}^{n_k \times d_k}$  such that  $[Y_k]_{i,\cdot} = y_{k,i}$ , and similarly introduce  $b_k := (b_{k,i})_{i=1}^{n_k} \in \Delta_{n_k}$ .

First, our objective is to re-write the iteration [Eq. \(10\)](#) in this discrete setting, with an initial measure  $\mu = \sum_{i=1}^n a_i \delta_{x_i} \in \mathcal{P}(\mathbb{R}^d)$ . For each  $k$ , we choose  $\pi_k \in \mathbb{R}_+^{n \times n_k}$  an optimal transport

plan, which is to say a solution of the Kantorovich linear program:

$$\operatorname{argmin}_{\Pi(a, b_k)} \sum_{i=1}^n \sum_{j=1}^{n_k} c_k(x_i, y_{k,j}) \pi_{i,j},$$

where  $\Pi(a, b_k) := \left\{ \pi \in \mathbb{R}_+^{n \times n_k} : \pi \mathbf{1} = a, \pi^T \mathbf{1} = b_k \right\}$ . Seeing multi-couplings  $\gamma \in \Gamma(\mu)$  as tensors  $\gamma \in \mathbb{R}^{n \times n_1 \times \dots \times n_k}$ , the discrete expression of  $G$  reads:

$$G(\mu) = \left\{ \sum_{j_1, \dots, j_K} \left( \sum_{i=1}^n \gamma_{1, j_1, \dots, j_K} \right) \delta(B(y_{1, j_1}, \dots, y_{K, j_K})) \right\}, \gamma \in \Gamma(\mu). \quad (22)$$

A visualisation of Eq. (22) using the multi-coupling from Eq. (9) is provided in Fig. 6.

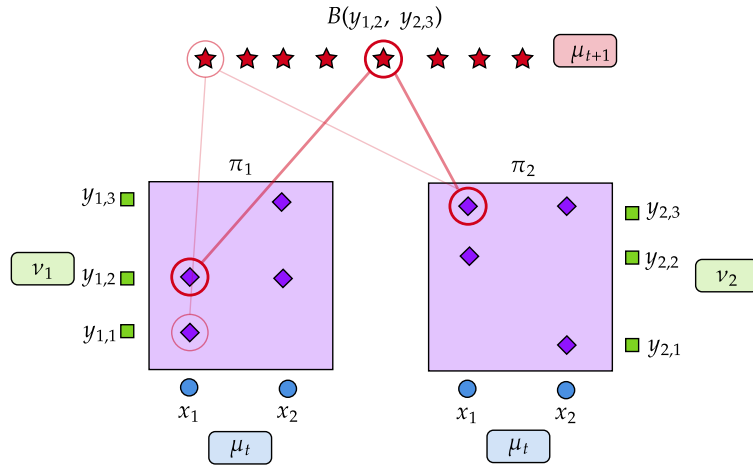


Figure 6: Visual explanation of the discrete fixed-point iteration  $G$ . For each point  $x_i$  in the support of  $\mu_t$ , we look at all the points  $(y_{1, j_1}, \dots, y_{K, j_K})$  which are assigned from  $x_i$  by the multi-coupling  $\gamma$ , then the ground barycentre  $B(y_{1, j_1}, \dots, y_{K, j_K})$  is taken on all these tuples, with weights given by the multi-coupling.

As in [BB25], we can use a generalisation of the North-West Corner (NWC) method to compute  $\gamma \in \Gamma(\mu)$  with prescribed bi-marginals  $\pi_k \in \Pi(a, b_k)$ . In Algorithm 1, we present the NWC strategy. The idea is to fill the entries of  $\gamma$  greedily using entries  $\pi_{i, j_k}^{(k)}$  for increasing  $i, j_1, \dots, j_K$  (see [PC19, Section 3.4.2] for a presentation of the method in the standard setting).

Noticing that Eq. (22) only requires the  $n_1 \times \dots \times n_K$ -tensor  $\rho := \gamma_{1, \dots, K}$ , it is possible to only store the indices  $(j_1, \dots, j_K)$  such that  $\rho_{j_1, \dots, j_K} > 0$ , as well as the corresponding weights  $\rho_{j_1, \dots, j_K}$ . This avoids the prohibitive memory cost of storing the full tensor  $\gamma$ , and takes advantage of the sparsity of the multi-coupling  $\gamma$ : if each  $\pi_k$  is an extremal point of  $\Pi(a, b_k)$ , we conjecture that  $\text{NWC}(\pi_1, \dots, \pi_K)$  is an extremal point of  $\Pi(a, b_1, \dots, b_K)$ , and thus  $\#\text{supp } \gamma \leq n + \sum_k n_k - K$  (adapting techniques from [ABM16, Theorem 2]).

Thanks to Eq. (22) we formalise the fixed-point iterations in the discrete case in Algorithm 2. Given our considerations on the support of NWC gluing, we expect (without formal proof) the upper bound  $\#\text{supp } \mu_T \leq n + T(\sum_k n_k) - TK$ . This is the same conclusion as [BB25], which they also state without proof about their Gromov-Wasserstein fixed-point iteration [BB25, Algorithm 5.2]. From a memory perspective, the algorithm does not require the storage of each  $\gamma \in \mathbb{R}^{N_t \times n_1 \times \dots \times n_K}$ , as remarked for the NWC algorithm.

In some specific cases, the expression in Eq. (22) becomes simpler. If the weights  $a$  and  $b_k$  are all uniform and  $n = n_1 = \dots = n_K$ , then the Birkhoff-von-Neumann Theorem allows the

**Algorithm 1:** North-West Corner Gluing.**Data:** For  $k \in \llbracket 1, K \rrbracket$ , transport plan  $\pi_k \in \Pi(a, b_k)$ , with  $a \in \Delta_n$  and  $b_k \in \Delta_{n_k}$ .**Result:** Gluing  $\text{NWC}(\pi_1, \dots, \pi_K) = \gamma \in \Pi(a, b_1, \dots, b_K)$  such that each  $\gamma_{0,k} = \pi_k$ .

```

1 Initialisation:  $\gamma = 0_{n \times n_1 \times \dots \times n_K}$  and for  $k \in \llbracket 1, K \rrbracket$ ,  $P_k = \pi_k$ .
2 for  $i \in \llbracket 1, n \rrbracket$  do
3   Set  $(j_1, \dots, j_K) = (1, \dots, 1)$  and  $u = a_i$ ;
4   while  $u > 0$  do
5     Compute  $v = \min(P_{i,j_1}^{(1)}, \dots, P_{i,j_K}^{(K)})$ ;
6     Assign  $\gamma_{i,j_1, \dots, j_K} = v$  and decrease  $u \leftarrow u - v$ ;
7     for  $k \in \llbracket 1, K \rrbracket$  do
8       Decrease  $P_{i,j_k}^{(k)} \leftarrow P_{i,j_k}^{(k)} - v$ ;
9       if  $P_{i,j_k}^{(k)} = 0$  then
10        Increment  $j_k \leftarrow j_k + 1$ ;
11      end
12    end
13  end
14 end

```

choice of each transport plan  $\pi_k$  as permutation assignments  $[\pi_k]_{i,j} = \frac{1}{n} \mathbb{1}(\sigma_k(i) = j)$ . In this case, the expression of  $G(\mu)$  becomes:

$$G(\mu) = \frac{1}{n} \sum_{i=1}^n \delta \left( B(y_{1,\sigma_1(i)}, \dots, y_{K,\sigma_K(i)}) \right). \quad (23)$$

If one takes the barycentric projections of the OT plans  $\pi^{(k)}$  in Eq. (22), one obtains a discrete expression of  $H$  (from Eq. (21)) written in Eq. (24) and visualised in Fig. 7.

$$H(\mu) = \left\{ \sum_{i=1}^n a_i \delta \left[ B \left( (1/a_i) \sum_{j=1}^{n_1} \pi_{i,j}^{(1)} y_{1,j}, \dots, (1/a_i) \sum_{j=1}^{n_K} \pi_{i,j}^{(K)} y_{K,j} \right) \right], \pi^{(k)} \in \Pi_{c_k}^*(\mu, \nu_k) \right\}. \quad (24)$$

Contrary to  $G$ , for  $H$  the number of points in the support of  $\mu_t$  remains the same, and the weights  $a$  remain fixed. In this setting, the optimisation is done solely on the positions, which can be seen as a Lagrangian formulation. Note that in the squared-Euclidean case, Eq. (24) is the formula proposed in [CD14, Equation 8] and **currently implemented** in the Python OT library [Fla+21]. A technical difference is that [CD14] also proposes an optimisation over the barycentre weights (by sub-gradient descent), while the fixed-point approach by [Álv+16] and ours do not. Furthermore, [CD14] suggests a computational simplification by using barycentric projections of *entropic* plans, for which, as for  $H$ , there are no theoretical guarantees (to our knowledge).

The practical advantage of the map-supported expressions in Eqs. (23) and (24) over Eq. (22) is computational: since the support size of  $\mu_t$  cannot increase, the cost of computing the OT plans at Line 4 is smaller. We shall see in Section 4.3 that in some cases, Kantorovich solutions are almost-surely permutations for random supports. While convenient, this expression only holds when all the measures have the same amount of points, in contrast to the barycentric expression Eq. (24).

We present the iteration of  $H$  as a cost-effective alternative to  $G$ , which is in some sense a simplification of the Block-Coordinate Descent (BCD) method, wherein the update with

---

**Algorithm 2:** Discrete iteration of  $G$ .

---

**Data:** barycentre coefficients  $(\lambda_k) \in \Delta_K$ , for  $k \in \llbracket 1, K \rrbracket$ , support of  $\nu_k$ :  $Y_k \in \mathbb{R}^{n_k \times d_k}$ , weights of  $\nu_k$ :  $b_k \in \Delta_{n_k}$  and cost function  $c_k : \mathbb{R}^d \times \mathbb{R}^{d_k} \rightarrow \mathbb{R}_+$ . Number of iterations  $T$ , initial size  $n \geq 1$  and stopping criterion  $\alpha \geq 0$ .

**Result:** Barycentre  $\mu_T = \sum_{i=1}^{N_t} a_i^{(T)} \delta_{x_i^{(T)}}$ .

```

1 Initialisation: Choose  $\mu_0 = \sum_{i=1}^n a_i^{(0)} \delta_{x_i^{(0)}}$  with  $a^{(0)} \in \Delta_n$  and  $X^{(0)} \in \mathbb{R}^{n \times d}$ .
2 for  $t \in \llbracket 0, T - 1 \rrbracket$  do
3   for  $k \in \llbracket 1, K \rrbracket$  do
4     | Solve the OT problem:  $\pi^{(k)} \in \operatorname{argmin}_{\pi \in \Pi(a^{(t)}, b_k)} \sum_{i,j} \pi_{i,j} c_k(x_i^{(t)}, y_{k,j})$ ;
5   end
6   Compute  $\gamma = \operatorname{NWC}(\pi^{(1)}, \dots, \pi^{(K)})$ ;
7   Compute  $\rho = \gamma_{1, \dots, K} = [\sum_i \gamma_{j_1, \dots, j_K}]_{j_1, \dots, j_K}$  and write  $\operatorname{supp} \rho = ((j_1^{(i)}, \dots, j_K^{(i)}))_{i=1}^{N_t}$ ;
8   for  $i \in \llbracket 1, N_t \rrbracket$  do
9     | Compute  $x_i^{(t+1)} = B(y_{1, j_1^{(i)}}, \dots, y_{K, j_K^{(i)}})$  and  $a_i^{(t+1)} = \rho_{j_1, \dots, j_K}$ ;
10  end
11  if  $W_2^2(\mu_{t+1}, \mu_t) < \frac{\alpha}{N_t} \|X^{(t)}\|_2^2$  then
12    | Declare convergence and terminate.
13  end
14 end
15 return  $a^{(T)}, X^{(T)}$ 

```

---

respect to the support  $X \in \mathbb{R}^{n \times d}$  with transport plans  $(\pi_k)$  fixed is done by computing:

$$X^* \in \operatorname{argmin}_{X \in \mathbb{R}^{n \times d}} \sum_{k=1}^K \sum_{i=1}^n \sum_{j=1}^{n_k} \pi_{i,j}^{(k)} c_k(x_i, y_{k,j}). \quad (25)$$

In practice, apart from the case of the squared Euclidean cost, the optimisation in Eq. (25) is not tractable, and one must resort to Gradient Descent (GD) methods. BCD methods with GD for the update of  $X$  can be seen as a variant of the full GD method which minimises  $X \mapsto V(\frac{1}{n} \sum_i \delta_{x_i})$ , and we leave their study for future work.

## 4.2 Correspondence of Gradient Descent with Fixed-Point Iterations

The fixed-point method of [Álv+16] applied to Bures-Wasserstein barycentres also corresponds to a gradient descent algorithm with a specific step size, as remarked by [Alt+21]. This also holds for discrete measures. Indeed, writing  $X = \{x_1, \dots, x_n\}$  and assuming  $\mu_X = \frac{1}{n} \sum_{i=1}^n \delta_{x_i}$ , an alternative to fixed-point iterations would be to apply a gradient descent directly on the non convex functional  $F : X \mapsto \sum_{k=1}^K \lambda_k \mathcal{T}_{c_k}(\mu_X, \nu_k)$ . For differentiable costs  $c_k$ , assuming that  $\nu_k = \frac{1}{n} \sum_{i=1}^n \delta_{y_{k,i}}$ , one step of such a gradient descent writes

$$\forall i \in \llbracket 1, n \rrbracket, x_i^{(t+1)} = x_i^{(t)} - \alpha \sum_{k=1}^K \lambda_k \nabla_x c_k(x_i^{(t)}, y_{k, \sigma_k^{(t)}(i)}), \quad (26)$$

where we choose an element of  $\Pi_{c_k}^*(\mu_{X^{(t)}}, \nu_k)$  induced by a permutation  $\sigma_k^{(t)}$  between  $\{x_1^{(t)}, \dots, x_n^{(t)}\}$  and  $\{y_{k,1}, \dots, y_{k,n}\}$ . The whole optimisation algorithm consists in alternating such gradient

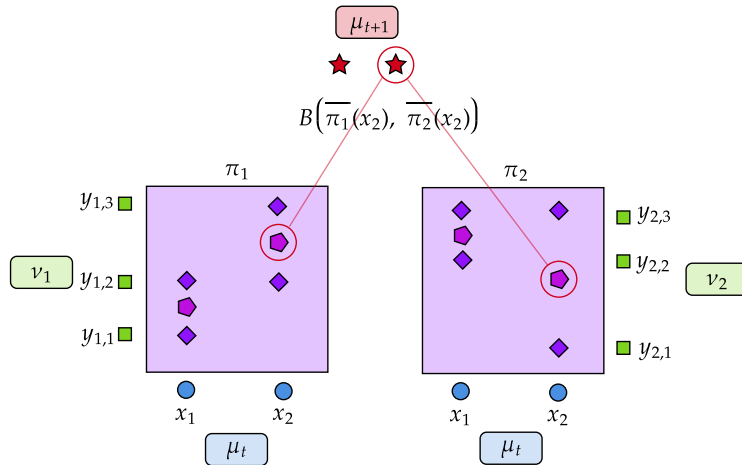


Figure 7: Visual explanation of the discrete fixed-point iteration  $H$ . For each point  $x_i$  in the support of  $\mu_t$  and  $k \in \llbracket 1, K \rrbracket$ , we look at all the points  $(y_{k,j_k})$  which are assigned from  $x_i$  by the OT plan  $\pi^{(k)}$  between  $\mu$  and  $\nu_k$ , then take their barycenter  $\bar{\pi}_k(x_i)$  (pentagons on the figure). The point  $x_i$  in the support of  $\mu_t$  is then sent to the point  $B(\bar{\pi}_1(x_i), \dots, \bar{\pi}_K(x_i))$  in  $\mu_{t+1}$ .

steps on  $X$  with updates of the optimal assignments  $\{\sigma_k^{(t)}\}$ , depending on the new point positions. In the fixed-point approach, this gradient step on each  $x_i^{(t)}$  is replaced by the computation of  $B(y_{1,\sigma_1^{(t)}(i)}, \dots, y_{K,\sigma_K^{(t)}(i)})$ , which corresponds to a full descent on  $X$  for a given configuration of assignments before updating the said assignments (in other words, alternate minimisation). For generic costs  $c_k$ , one may also use a gradient descent strategy to compute barycentres  $B(y_{1,\sigma_1^{(t)}(i)}, \dots, y_{K,\sigma_K^{(t)}(i)})$ , that is gradient descents on the  $K$  functionals  $x \mapsto \sum_{k=1}^K c_k(x, y_{k,\sigma_k^{(t)}(i)})$ , and such descents write exactly as Eq. (26). In this case, the only difference between both approaches is that the fixed point algorithm applies the whole descent on  $X$  before updating assignments, while gradient descent on  $F$  alternates steps of gradient descent on  $X$  with updates of the assignments.

When  $c_k = \|\cdot - \cdot\|_2^2$ , both approaches are equivalent if the gradient step is chosen as  $\alpha = \frac{1}{2}$ . Indeed, a gradient iteration on  $F$  writes

$$\forall i \in \llbracket 1, n \rrbracket, x_i^{(t+1)} = (1 - 2\alpha)x_i^{(t)} + 2\alpha \sum_{k=1}^K \lambda_k y_{k,\sigma_k^{(t)}(i)} = \sum_{k=1}^K \lambda_k y_{k,\sigma_k^{(t)}(i)}.$$

It follows that for  $\alpha = \frac{1}{2}$ , one step of gradient descent computes directly the barycentre for the current configuration of assignments  $\{\sigma_k^{(t)}\}$ , which is precisely one iteration of the fixed-point algorithm. For different cost functions, similar optimal steps may be formulated, but the step may depend on  $i$  and  $x_i^{(t)}$ .

Choosing the best strategy between the fixed point approach and the gradient descent surely depends on the set of costs. When  $B$  is easily computable (more efficiently than by gradient descent), the fixed point algorithm moves the points faster than gradient descent. However, it is not obvious what should be the better option for complex costs  $c_k$  in practice. More generally, one could wonder if updating assignments more often (which is the case for the gradient descent on  $F$ ) might not help avoiding local minima of the whole functional which is non convex in  $X$ . We did not observe this behaviour in practice in our experiments and therefore recommend the fixed point approach as the default choice.

**Algorithm 3:** Discrete iteration of  $H$ .

**Data:** barycentre coefficients  $(\lambda_k) \in \Delta_K$ , for  $k \in \llbracket 1, K \rrbracket$ , support of  $\nu_k$ :  $Y_k \in \mathbb{R}^{n_k \times d_k}$ , weights of  $\nu_k$ :  $b_k \in \Delta_{n_k}$  and cost function  $c_k : \mathbb{R}^d \times \mathbb{R}^{d_k} \rightarrow \mathbb{R}_+$ . Number of iterations  $T$ , barycentre size  $n \geq 1$ , weights  $a \in \Delta_n$  and stopping criterion  $\alpha \geq 0$ .

**Result:** Barycentre  $\mu_T = \sum_{i=1}^n a_i \delta_{x_i^{(T)}}$ .

```

1 Initialisation: Choose  $\mu_0 = \sum_{i=1}^n a_i \delta_{x_i^{(0)}}$  with  $X^{(0)} \in \mathbb{R}^{n \times d}$ .
2 for  $t \in \llbracket 0, T - 1 \rrbracket$  do
3   for  $k \in \llbracket 1, K \rrbracket$  do
4     | Solve the OT problem:  $\pi^{(k)} \in \operatorname{argmin}_{\pi \in \Pi(a, b_k)} \sum_{i,j} \pi_{i,j} c_k(x_i^{(t)}, y_{k,j})$ ;
5   end
6   for  $i \in \llbracket 1, n \rrbracket$  do
7     | Compute  $x_i^{(t+1)} = B\left((1/a_i) \sum_{j=1}^{n_1} \pi_{i,j}^{(1)} y_{1,j}, \dots, (1/a_i) \sum_{j=1}^{n_K} \pi_{i,j}^{(K)} y_{K,j}\right)$ ;
8   end
9   if  $W_2^2(\mu_{t+1}, \mu_t) < \frac{\alpha}{n} \|X^{(t)}\|_2^2$  then
10    | Declare convergence and terminate.
11  end
12 end
13 return  $X^{(T)}$ 

```

### 4.3 Discrete Uniqueness Discussion

In this section, we investigate conditions to have uniqueness in the discrete Kantorovich problem between measures  $\mu = \sum_{i=1}^{n_x} a_i \delta_{x_i} \in \mathcal{P}(\mathbb{R}^{d_x})$  and  $\nu = \sum_{j=1}^{n_y} b_j \delta_{y_j} \in \mathcal{P}(\mathbb{R}^{d_y})$ :

$$\min_{\pi \in \Pi(a, b)} \sum_{i=1}^{n_x} \sum_{j=1}^{n_y} \pi_{i,j} c(x_i, y_j). \quad (27)$$

For convenience, we introduce  $X := (x_1, \dots, x_{n_x}) \in \mathbb{R}^{n_x \times d_x}$  and  $Y := (y_1, \dots, y_{n_y}) \in \mathbb{R}^{n_y \times d_y}$ . The following result shows that if the cost matrix  $M := (X, Y) \mapsto (c(x_i, y_j))_{i,j} \in \mathbb{R}^{n_x \times n_y}$  is not orthogonal to a face of the transportation polytope, then the discrete Kantorovich problem has a unique solution. For convenience, we write  $\pi \cdot M := \sum_{i,j} \pi_{i,j} M_{i,j}$ .

**Proposition 4.1.** *Let  $a \in \Delta_{n_x}$  and  $b \in \Delta_{n_y}$  be fixed weights and  $c : \mathbb{R}^{d_x} \times \mathbb{R}^{d_y} \rightarrow \mathbb{R}_+$  a cost function. Consider the cost matrix function*

$$M := \begin{cases} \mathbb{R}^{n_x \times d_x} \times \mathbb{R}^{n_y \times d_y} & \longrightarrow & \mathbb{R}^{n_x \times n_y} \\ (X, Y) & \longmapsto & (c(x_i, y_j))_{i,j} \end{cases},$$

and let  $(X, Y) \in \mathbb{R}^{n_x \times d_x} \times \mathbb{R}^{n_y \times d_y}$ . Denote by  $\operatorname{Extr} \Pi(a, b)$  the (finite) set of extremal points of the transportation polytope  $\Pi(a, b)$ .

$$\min_{\pi \in \Pi(a, b)} \pi \cdot M(X, Y) \text{ has a unique solution} \iff M(X, Y) \notin \bigcup_{\pi_1 \neq \pi_2 \in \operatorname{Extr} \Pi(a, b)} (\pi_1 - \pi_2)^\perp. \quad (28)$$

**Proof.** Since  $\Pi(a, b)$  is convex and compact in  $\mathbb{R}^{n_x \times n_y}$ , by the Krein-Milman theorem, it is the convex hull of the set of its extreme points, denoted  $\text{Extr} \Pi(a, b)$ . With the definition

$$\Pi(a, b) = \left\{ \pi \in \mathbb{R}^{n_x \times n_y} : \pi \geq 0, \pi \mathbf{1} = a, \pi^T \mathbf{1} = b \right\},$$

we see that  $\Pi(a, b)$  is a polytope, and thus  $\text{Extr} \Pi(a, b)$  is finite. Since the Kantorovich problem is a linear problem, the set of optimal solutions is exactly the set of convex combinations of optimal extremal points. As a result, we have non-uniqueness in Eq. (27) if and only if there exists  $\pi_1 \neq \pi_2 \in \text{Extr} \Pi(a, b) : \pi_1 \cdot M(X, Y) = \pi_2 \cdot M(X, Y)$ . We conclude that uniqueness holds if and only if  $\forall \pi_1 \neq \pi_2 \in \text{Extr} \Pi(a, b) : M(X, Y) \notin (\pi_1 - \pi_2)^\perp$ .  $\square$

A consequence of Proposition 4.1 is that if  $M \# \mathcal{L}^{n_x \times d_x + n_y \times d_y}$  does not give mass to hyperplanes of  $\mathbb{R}^{n_x \times n_y}$ , then the Kantorovich problem has a unique solution for  $\mathcal{L}^{n_x \times d_x + n_y \times d_y}$ -almost-every  $(X, Y)$ . Furthermore, if the measures have the same amount of points ( $n_x = n_y$ ) and the weights are uniform, then the extreme points of  $\Pi(a, b)$  are permutations, which provides a theoretical justification for the convenient expression in Eq. (23).

#### 4.4 Application to Gaussian Mixture Model Barycentres

In this section, we explain how our fixed-point algorithm can be applied to compute barycentres between Gaussian Mixture Models (GMMs), providing a new numerical method for the GMM barycentre notion introduced in [DD20, Section 5]. The notation  $S_d^{++}(\mathbb{R})$  will refer to the cone of positive definite symmetric  $d \times d$  matrices.

We consider the case where the measures are Gaussian Mixture Models, seen as discrete measures over the space of Gaussian measures on  $\mathbb{R}^d$ :  $\mathcal{X} := \mathcal{N} := \left\{ \mathcal{N}(m, S) : m \in \mathbb{R}^d, S \in S_d^{++}(\mathbb{R}) \right\}$ , equipped with the 2-Wasserstein distance, which has a specific expression called the *Bures-Wasserstein distance*:

$$W_2^2(\mathcal{N}(m_1, S_1), \mathcal{N}(m_2, S_2)) = \|m_1 - m_2\|_2^2 + \underbrace{\text{Tr} \left( S_1 + S_2 - 2(S_1^{1/2} S_2 S_1^{1/2})^{1/2} \right)}_{d_{\text{BW}}^2(S_1, S_2)}. \quad (29)$$

Alternatively, one could see the same problem differently, setting  $\mathcal{X} := \mathbb{R}^d \times S_d^{++}(\mathbb{R})$  equipped with the distance defined in Eq. (29). To remind the definition of barycentres between Gaussian mixture models from [DD20], we will consider measures that lie on the same space of Gaussian measures:  $\mathcal{X} = \mathcal{Y}_1 = \dots = \mathcal{Y}_K = \mathcal{N}$ . Next, we choose cost functions  $c_k$  on  $\mathcal{N}$  as the squared Bures-Wasserstein distance  $W_2^2$  scaled by  $\lambda_k$ . Given mixture models  $\mu, \nu \in \mathcal{P}(\mathcal{N})$  of the form

$$\mu = \sum_{i=1}^n a_i \delta_{\mathcal{N}(m_i, S_i)}, \quad \nu = \sum_{j=1}^m b_j \delta_{\mathcal{N}(m'_j, S'_j)},$$

the Optimal Transport cost  $\mathcal{T}_{W_2^2}(\mu, \nu)$  is the value of a discrete problem, which is precisely the Mixed Wasserstein Distance introduced in [DD20, Proposition 4]:

$$\mathcal{T}_{W_2^2}(\mu, \nu) = \min_{\pi \in \Pi(a, b)} \sum_{i, j} \pi_{i, j} W_2^2(\mathcal{N}(m_i, S_i), \mathcal{N}(m'_j, S'_j)). \quad (30)$$

Consider  $K$  GMM measures  $\nu_k$  written as:

$$\nu_k = \sum_{j=1}^{n_k} b_{k, j} \delta_{\mathcal{N}(m_{k, j}, S_{k, j})} \in \mathcal{P}(\mathcal{N}),$$

their GMM barycentre cost with weights  $(\lambda_k)$  for  $\mu = \sum_{i=1}^n a_i \delta_{\mathcal{N}(m_i, S_i)} \in \mathcal{P}(\mathcal{N})$  reads:

$$V(\mu) = \sum_{k=1}^K \lambda_k \min_{\pi_k \in \Pi(a, b_k)} \sum_{i,j} \pi_{i,j} \left( \|m_i - m_{k,j}\|_2^2 + d_{\text{BW}}^2(S_i, S_{k,j}) \right). \quad (31)$$

We now turn to the expression of the ground barycentre function  $B : \mathcal{N}^K \rightarrow \mathcal{N}$ . This corresponds to a 2-Wasserstein barycentre problem in the Gaussian case, which was first studied by [AC11] (showing existence and uniqueness in [AC11, Theorem 6.1]):

$$B(\mathcal{N}(m_1, S_1), \dots, \mathcal{N}(m_K, S_K)) = \mathcal{N}(\bar{m}, \bar{S}), \quad \bar{m} := \sum_{k=1}^K \lambda_k m_k, \quad \bar{S} := \operatorname{argmin}_{S \in S_d^{++}(\mathbb{R})} \sum_{k=1}^K \lambda_k d_{\text{BW}}^2(S, S_k).$$

A fixed-point formulation of this problem is presented in [Álv+16] as a particular case of their study of the fixed-point algorithm for the ground cost  $\|\cdot - \cdot\|_2^2$  and absolutely continuous measures. This problem is presented again in [BJL17], where they prove additional convergence guarantees. We recall from [Álv+16; BJL17] the fixed-point algorithm to compute the barycentre of  $K$  Gaussians  $(\mathcal{N}(m_k, S_k))$  and weights  $(\lambda_1, \dots, \lambda_K)$ , which consists in iterating the function  $G_{\mathcal{N}} : S_d^{++}(\mathbb{R}) \rightarrow S_d^{++}(\mathbb{R})$ :

$$G_{\mathcal{N}}(S) = S^{-1/2} \left( \sum_{k=1}^K \lambda_k (S^{1/2} S_k S^{1/2})^{1/2} \right)^2 S^{-1/2}. \quad (32)$$

Now that we have defined the ground barycentre map  $B$ , we can apply our fixed-point algorithm to compute a barycentre. Given a reference GMM with  $n$  components  $\mu = \sum_{i=1}^n a_i \delta_{\mathcal{N}(m_i, S_i)}$ , for  $k \in \llbracket 1, K \rrbracket$ , solve the discrete Kantorovich problem between  $\mu$  and  $\nu_k$  (Eq. (30)) and choose  $\pi_k \in \Pi_{\mathbb{W}_2^*}^*(\mu, \nu_k)$ . The GMM of  $G(\mu)$  associated to the choice of plans  $\pi_k \in \Pi(a, b_k)$  in the iteration scheme is the GMM  $\bar{\mu}$  defined by:

$$\bar{\mu} = \sum_{j_1, \dots, j_K} \sum_{i=1}^n \frac{1}{a_i^{K-1}} \pi_{i, j_1}^{(1)} \times \dots \times \pi_{i, j_K}^{(K)} \delta[B(\mathcal{N}(m_{1, j_1}, S_{1, j_1}), \dots, \mathcal{N}(m_{K, j_K}, S_{K, j_K}))].$$

As we argued in Section 4.1, it is computationally wise to consider a variant of the fixed-point iterations which use the barycentric projections of the couplings  $\pi_k$  (see Eq. (21)). To use this in the case of the space  $\mathcal{N}$ , we need to choose a notion of convex combination in  $\mathcal{N}$  to be able to compute the images of the barycentric projections. The most meaningful choice is a Wasserstein Gaussian barycentre, which corresponds to using the ground barycentre map  $B$  (this time with weights given by the disintegration of the coupling in question).

**Remark 4.2.** *The metric space  $(\mathcal{N}, \mathbb{W}_2)$  is not compact, however we consider discrete measures (GMMs). We will show how one can restrict  $\mathcal{N}$  to a compact subset containing all barycentres. Combining [DD20, Corollary 3] and [Álv+16, Theorem 4.2, Equations 20 and 21], shows that the barycentre is within a certain compact subset of  $\mathcal{P}(\mathcal{N})$  of measures supported on Gaussians with covariances whose eigenvalues are in a segment  $[r, R]$ , where  $0 < r < R$  are explicit constants depending on the covariances of the components of  $\nu_1, \dots, \nu_K$ . As for the means, they can be constrained to the convex hull of the means of the components of the mixtures  $\nu_k$ .*

## 5 Numerical Illustrations

In this section, we provide numerical experiments to illustrate the fixed-point method (specifically its barycentric variant presented in Algorithm 3) on various toy datasets. All code from

this section is available [in our companion Python toolkit](#). A numerical implementation of [Algorithm 2](#), which allows flexible support sizes, is also possible, but computationally much less appealing than [Algorithm 3](#).

## 5.1 Toy Example for Barycentre Computation

We begin with a simple example of barycentre computation in  $\mathbb{R}^2$  of two discrete uniform measures with different support sizes and for the square-Euclidean cost  $c_k(x, y) = \|x - y\|_2^2$ . We observe convergence to the true barycentre in two iterations in [Fig. 8](#). The support size increases from 10 to 19 at the first iteration and remains at 19 at the final iteration.

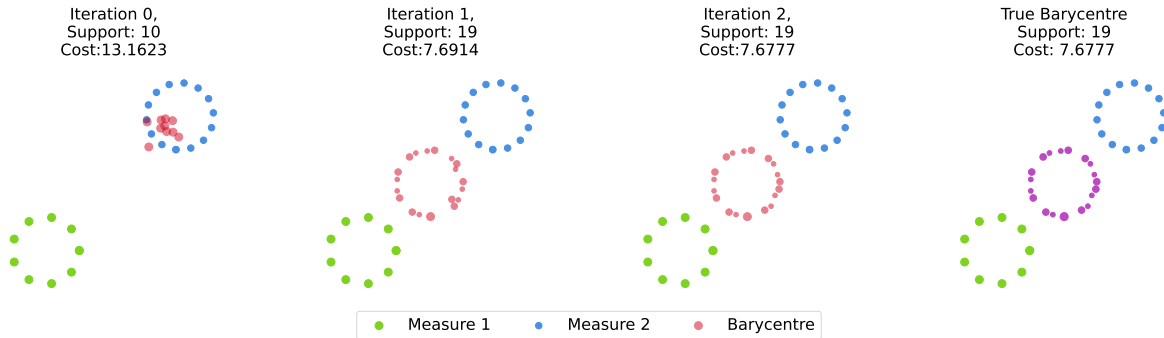


Figure 8: Iterations of [Algorithm 2](#) for the square-Euclidean cost, and comparison with the true  $W_2^2$  barycentre.

## 5.2 Illustration with Norm Powers

We consider discrete measures in  $\mathbb{R}^2$  for costs  $c_k(x, y) = \|x - y\|_p^q$ , as illustrated in [Fig. 9](#).

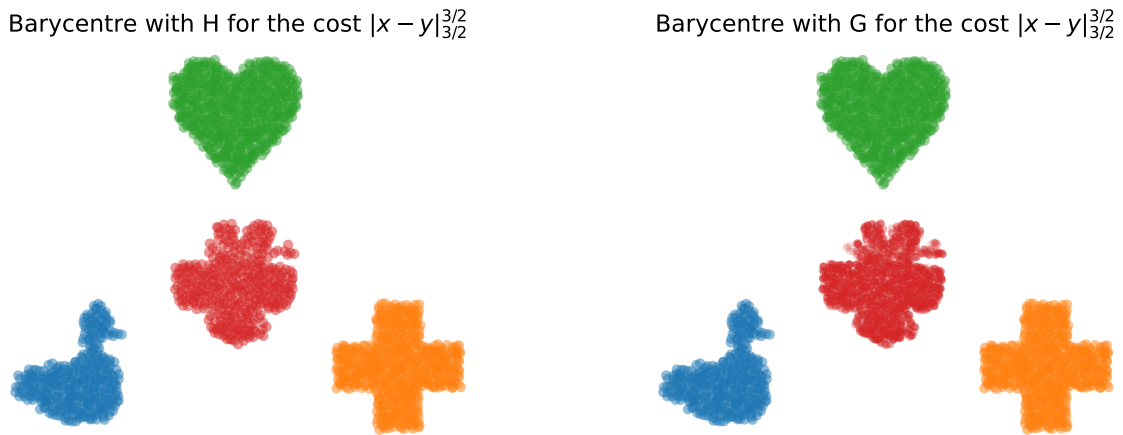


Figure 9: Barycentres with initial support size  $n = 400$  for  $(p, q) = (\frac{3}{2}, \frac{3}{2})$  of three measures with sizes 561, 382, 629.

In [Fig. 10](#), we observe that for  $(p, q) = (\frac{3}{2}, \frac{3}{2})$ , the iterates of  $G$  ([Algorithm 2](#)) have an energy that converges in one iteration, but the support size continues to grow at iteration 2. As for  $H$  ([Algorithm 3](#)), we observe in [Fig. 11](#) convergence in one iteration. In [Fig. 12](#), we present barycentres for various pairs  $(p, q)$  using iterates of  $H$ .

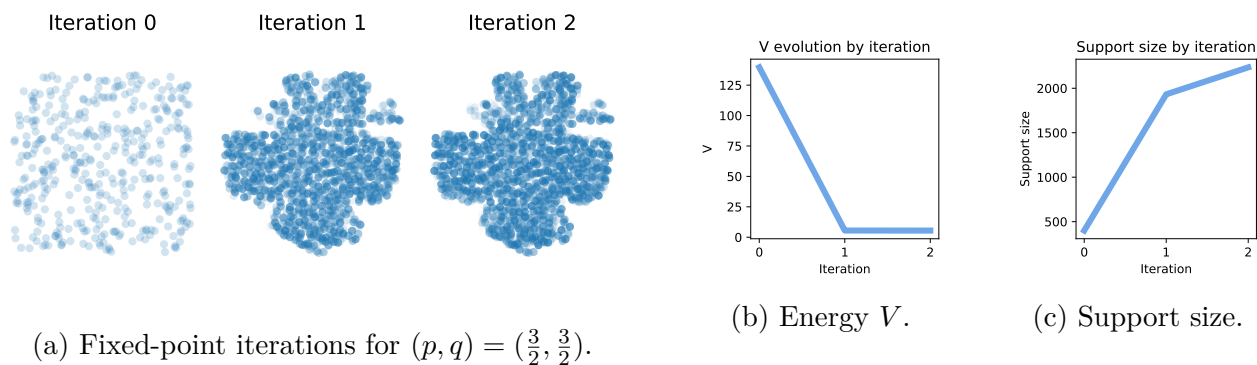


Figure 10: Convergence of the iterations of  $G$  (Algorithm 2).

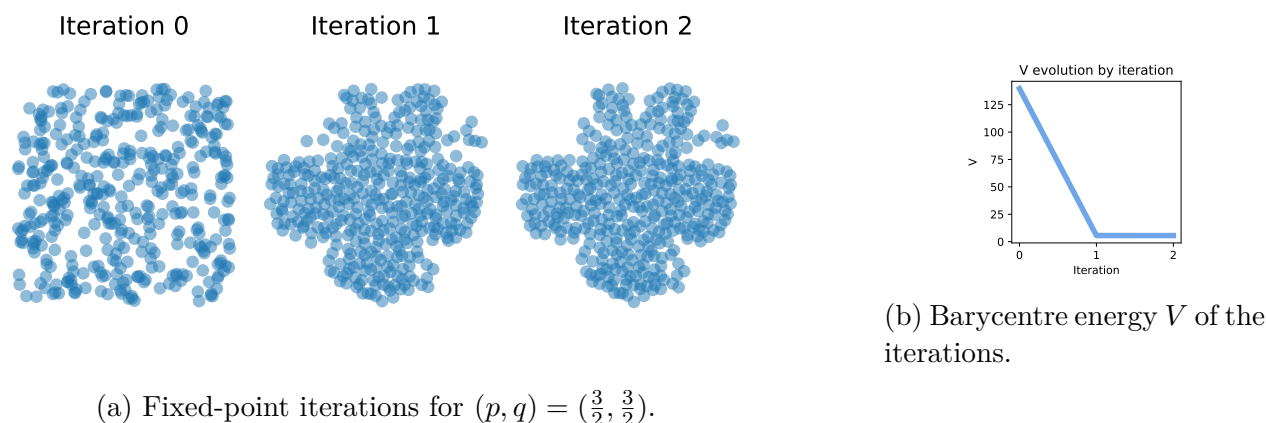


Figure 11: Convergence of the iterations of  $H$  (Algorithm 3).

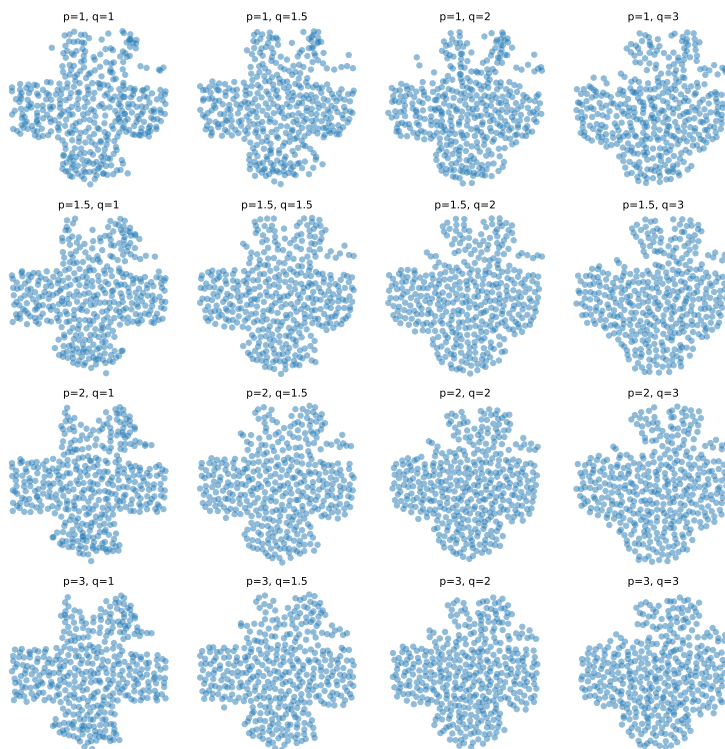


Figure 12: Barycentres for the cost  $\|x - y\|_p^q$  for different values of  $(p, q)$ .

In the following, we consider a different setting where two of the three target measures are identical, and with a different third target. This will allow us to study the robustness properties of the associated barycentre, seeing the third different measure as an outlier. We represent the target measures and a barycentre in Fig. 13, and compare different barycentres varying the parameters  $(p, q)$  of the cost  $\|\cdot - \cdot\|_p^q$  in Fig. 14. We observe that the barycentre obtained for  $q = 1$  always takes the shape of the duck, as this power allows for greater robustness to outliers (here the heart-shaped cloud), regardless of the norm. The influence of the third point cloud becomes increasingly evident as  $p$  and  $q$  grow.

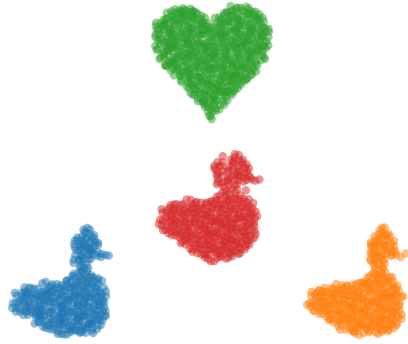


Figure 13: Barycentre of three point clouds for the cost  $\|\cdot - \cdot\|_{3/2}^{3/2}$ .

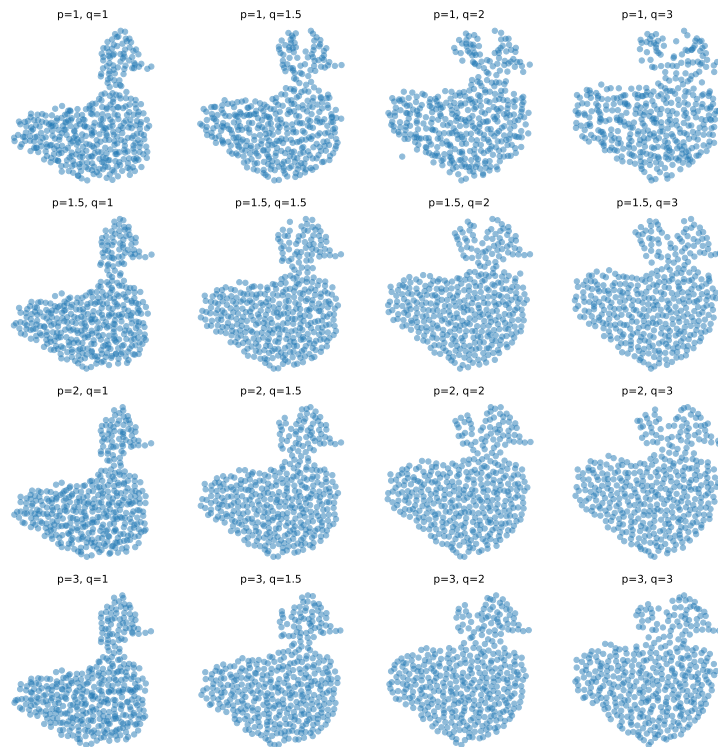


Figure 14: Barycentres for the measures of figure 13, for norms  $p$  raised to the power  $q$ .

### 5.3 Study of the Support Size of Iterates of $G$

In this section, we study the support size  $N$  of the final iteration of  $G$  (Algorithm 2). As discussed in Section 4.1, we expect (without formal proof) that the support size after  $T$  iterations is upper-bounded by  $N_0 + T \sum_k n_k - TK$ , where  $N_0$  is the initial support size and

$n_k$  is the size of the  $k$ -th marginal. We verify this hypothesis on numerical experiments on numerous configurations varying  $N_0, (n_k), d, (d_k)$  with measure points and weights generated randomly and for the square-Euclidean cost in Fig. 15. We observe that the upper-bound is indeed respected, and that the algorithm attains convergence in a small number of iterations.

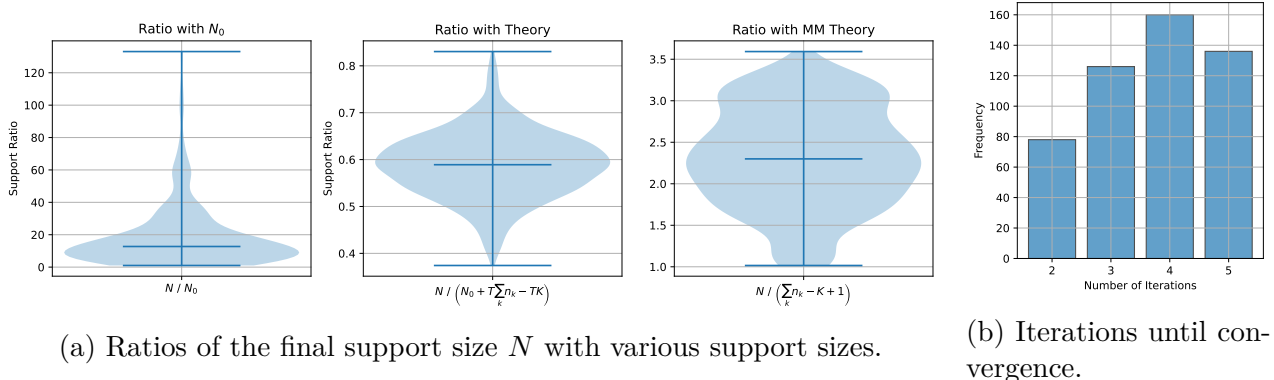


Figure 15: Numerical study of the support size  $N$  of iterates of  $G$ . We ran 500 samples, each drawing a random number of measures  $K \in \llbracket 2, 10 \rrbracket$ , random dimensions  $d, d_1, \dots, d_K \in \llbracket 1, 20 \rrbracket$ , random initial support sizes  $N_0 \in \llbracket 10, 100 \rrbracket$  and random measure sizes  $n_k \in \llbracket 10, 100 \rrbracket$ .

Running the same experiment as in Fig. 15 with  $N_0 = n_1 = \dots = n_K$  and uniform measure weights, we obtain, as expected in Eq. (23) that the support size  $N_t$  remains constant.

## 5.4 Comparison with the Multi-Marginal Formulation

Following Eq. (7), the discrete OT barycentre problem has a multi-marginal formulation, which can be written as follows, given measures  $\nu_k = \sum_{j=1}^{m_k} b_{k,j} \delta_{y_{k,j}}$ :

$$\operatorname{argmin}_{\pi \in \Pi(b_1, \dots, b_K)} \sum_{j_1, \dots, j_K} \pi_{j_1, \dots, j_K} \sum_{k=1}^K c_k(B(y_{1,j_1}, \dots, y_{K,j_K}), y_{k,j_k}). \quad (33)$$

Numerical solvers for Eq. (33), while slow, allow the computation of the exact solution of the barycentre problem. Comparing this solution to the output of our algorithm is technical, since the barycentric version of our algorithm imposes the size of the support of the barycentre in addition to imposing the weights, which introduces bias. We aim to illustrate that the speed of the barycentric algorithm, with a quantitative study of the error with respect to the multi-marginal “ground truth”. Note that even in this square-euclidean experiment, there is no widespread multi-marginal solver, which is why we also contribute an implementation.

The experimental setup is the following: the  $K$  measures  $\nu_k$  are all uniform measures with  $n$  points in  $\mathbb{R}^d$  drawn independently from  $\mathcal{N}(0, 1)$ . For the fixed-point algorithm, the initial measure is also taken as a uniform measure over  $n$  points with  $\mathcal{N}(0, 1)$  samples. We compare different numbers of iterations of the fixed-point algorithm and different choices of  $n, d, K$ . The plots show the ratios of the energy  $V$  and computation times for our algorithm divided by a Linear Programming multi-marginal solver, plotting 30% and 70% quantiles across 10 samples for each configuration. As expected in Eq. (23), since in this case the measures are uniform with a common support size, the iterates of  $H$  and  $G$  are identical in this setting.

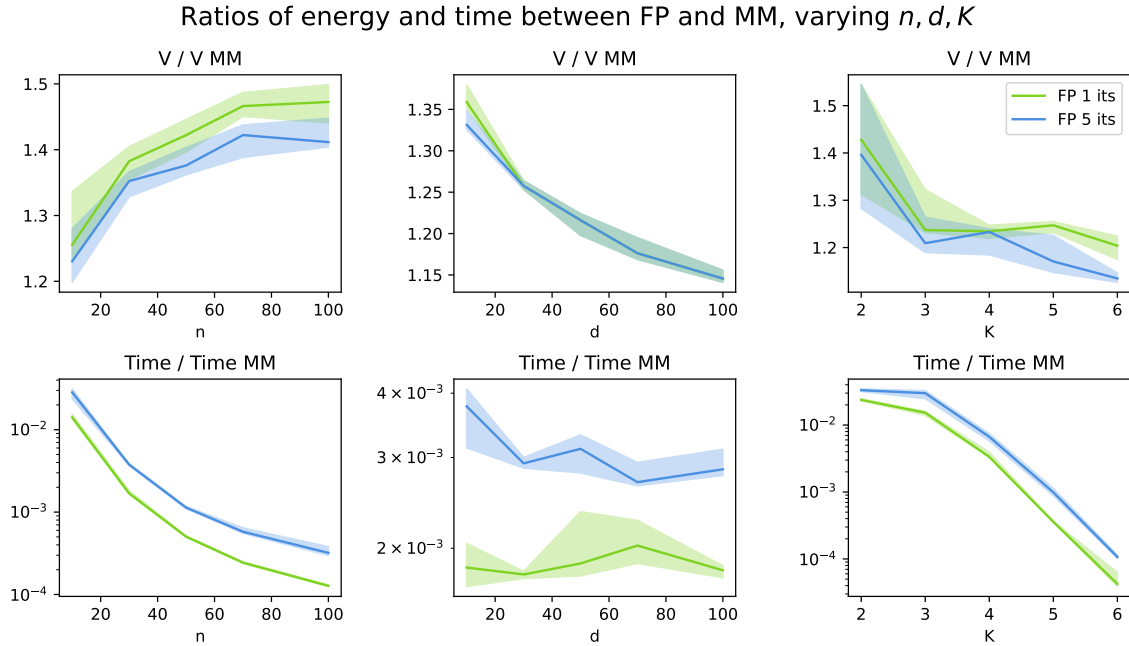


Figure 16: Comparing the fixed-point solver with a linear programming multi-marginal solver. From left to right columns: varying  $n$  with  $d = 10$  and  $K = 3$ ; varying  $d$  with  $n = 30$  and  $K = 3$ ; varying  $K$  with  $n = 10$  and  $d = 10$ . The comparison is made by dividing the energy value  $V$  (resp. computation time) of the fixed-point solution by the multi-marginal solution. The different curves correspond to  $T = 1, 5, 10$  iterations (legend in the top-right).

From the results presented in Fig. 16, it appears that the fixed-point algorithm converges in very few iterations, has an energy at most 50% worse than the exact multi-marginal solution, and is orders of magnitude faster, especially for larger measure sizes  $n$  and for greater numbers of marginals  $K$ . Note that for  $n \geq 10$  and  $K \geq 10$  for example, the multi-marginal problem is computationally intractable.

To compare with similar barycentre support sizes, in Fig. 17 we experiment with fixed-point barycentres using  $H$  (Algorithm 3) with  $N_{\text{FP}} = (n-1)K + 1$  points. The rationale behind this choice stems from the fact that discrete measures with  $n_1, \dots, n_K$  points have a barycentre with at most  $\sum_k n_k - K + 1$  points ([ABM16, Theorem 2]<sup>4</sup>).

<sup>4</sup>whose techniques are in fact not specific to the cost  $\|\cdot - \cdot\|_2^2$

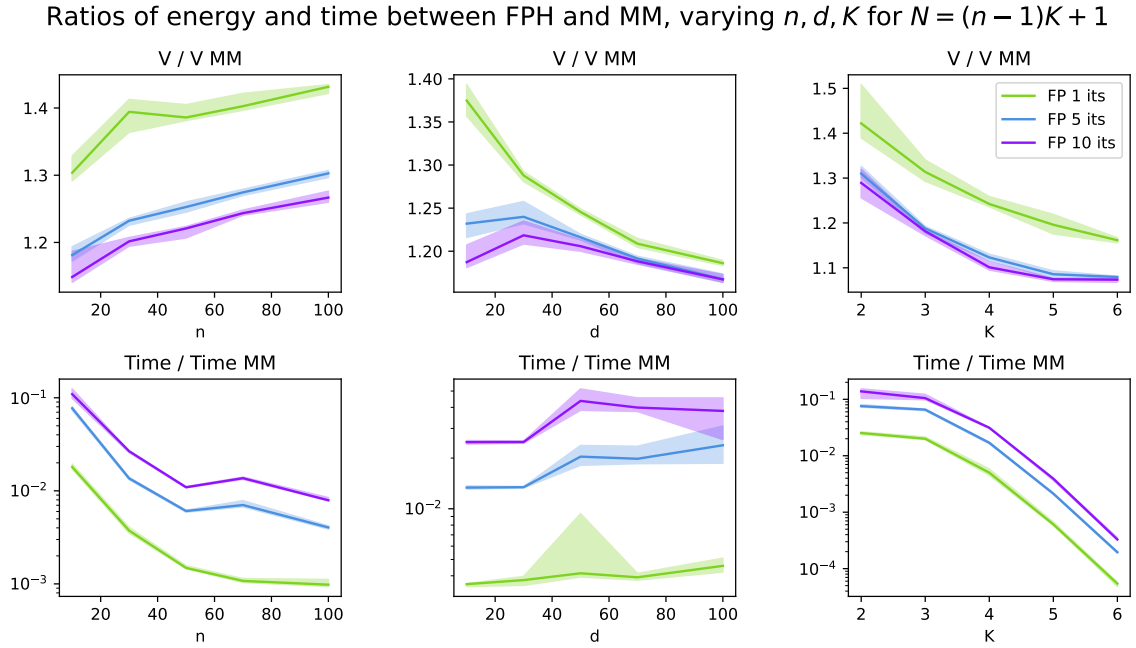


Figure 17: Comparing the fixed-point solver from [Algorithm 3](#) for  $N_{\text{FP}} = (n - 1)K + 1$  and the same setup as in [Fig. 16](#).

We now focus on the iterations of  $G$  ([Algorithm 2](#)) in the case of uniform measures where the initialisation is taken with  $n$  points and the target measures have even spaced sizes  $n_1 = \frac{n}{2} \cdots n_K = 2n$ . This ensures that iterates of  $G$  differ from iterates of  $H$ , and we present the results in [Fig. 18](#).

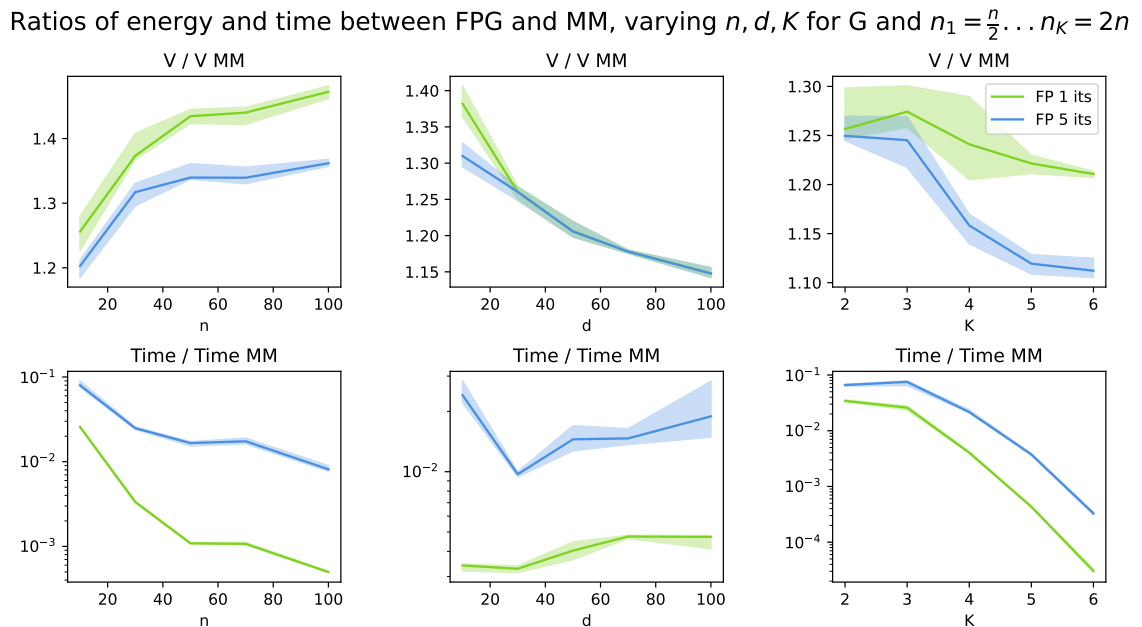


Figure 18: Comparing the fixed-point solver from [Algorithm 2](#) with the MM solver, for an initialisation with  $n$  points and target measures with different sizes  $n_1 = \frac{n}{2} \cdots n_K = 2n$ .

[Figs. 16 to 18](#) suggests that the fixed-point methods proposed in [Algorithms 2](#) and [3a](#) are useful as fast approximate solvers for the barycentre problem, and that settings with larger barycentre supports may require more iterations to converge. The main takeaway is that

our methods remain competitive for large supports and number of target measures, yet its convergence speed and overall advantages are more pronounced for smaller supports.

## 5.5 Generalised Wasserstein Barycentre Computation

In Fig. 19a, we illustrate the case where  $c_k(x, y) = \|P_k x - y\|_2$ , where  $P_k : \mathbb{R}^3 \rightarrow \mathbb{R}^2$  is an orthogonal projection. The problem finds a 3D measure whose projections attempt to match the reference 2D measures, which we compare in Fig. 19b. This is a modification of the exponent 2 from Generalised Wasserstein Barycentres [DGS21].

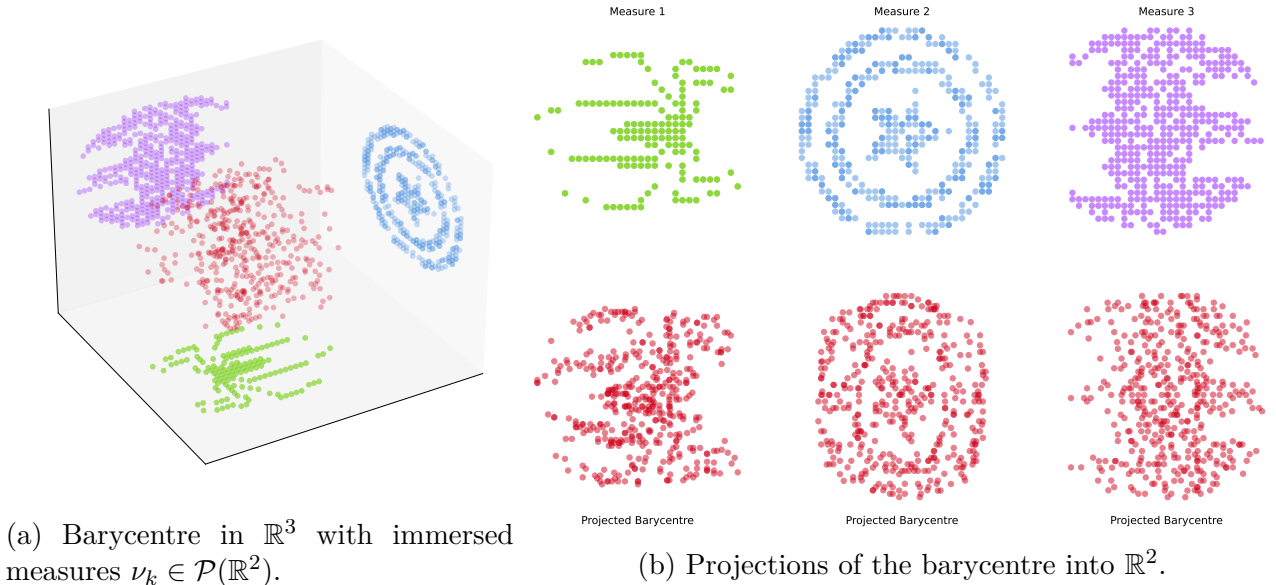


Figure 19: Barycenter (using Algorithm 3) with costs  $c_k(x, y) = \|P_k x - y\|_2$ , where  $P_k$  are orthogonal projections from  $\mathbb{R}^3$  to the three axes-aligned planes of the orthonormal basis. We provide an animation in the companion code.

## 5.6 Non-linear Generalised Wasserstein Barycentre Computation

In this illustration, we look for a barycenter in  $\mathbb{R}^2$  whose projections onto different circles match measures on these circles. We choose the costs  $c_k(x, y) = \|P_k(x) - y\|_2^2$ , where  $P_k$  is the projection onto the circle  $k$ . Since  $P_k$  is not linear, this is a direct generalisation of [DGS21].

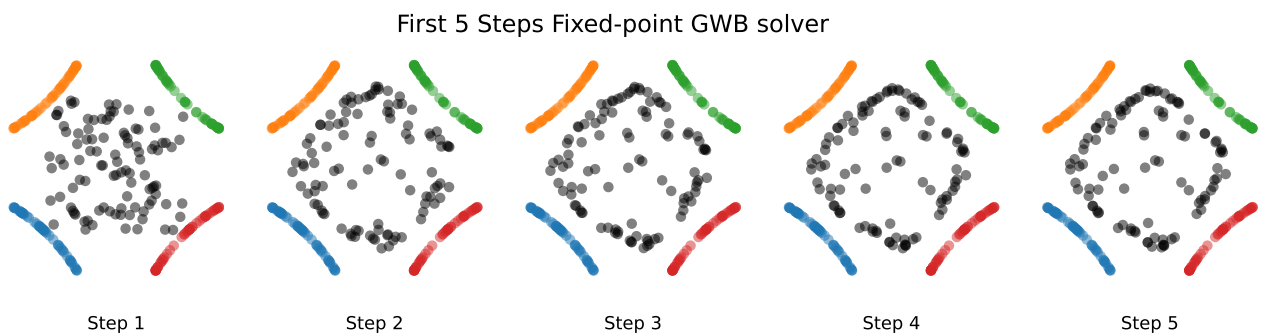


Figure 20: First 5 iterations of the fixed-point algorithm (Algorithm 3) for costs  $c_k(x, y) = \|P_k(x) - y\|_2^2$ , where  $P_k$  are projections onto four different circles on which the  $\nu_k$  are supported (plotted in colour).

In this instance, convergence happens quickly, but a stationary point is only reached after about 5 iterations, as observed on the steps in [Fig. 20](#) and on the energy curve in [Fig. 21](#).

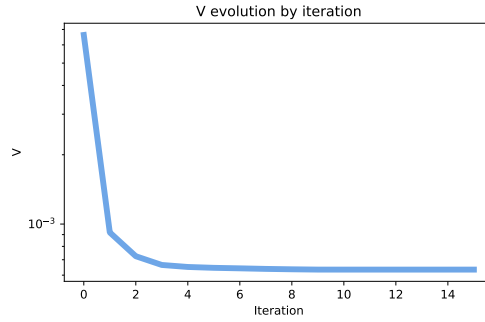


Figure 21: Barycentre energy  $V$  of the fixed-point algorithm for  $H$  across iterations.

## 5.7 Gaussian Mixture Model Barycentres

We illustrate numerical solutions of the GMM Barycentre method introduced in [Section 4.4](#). In [Fig. 22](#), we compare the multi-marginal solution with the output of our algorithm (we use [Algorithm 3](#)).

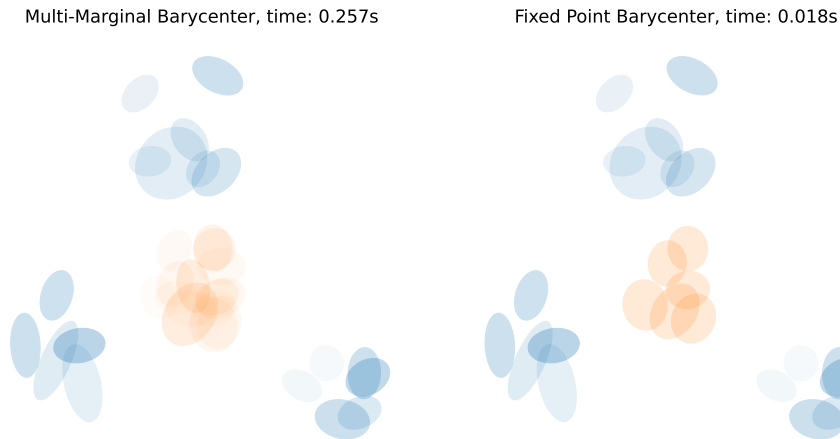


Figure 22: Left: multi-marginal solution for the GMM barycentre problem. Right: fixed-point solution for  $n = 6$  components.

Finally, in [Fig. 24](#) we illustrate barycentres between 4 GMMs shown in [Fig. 23](#) with different weights.

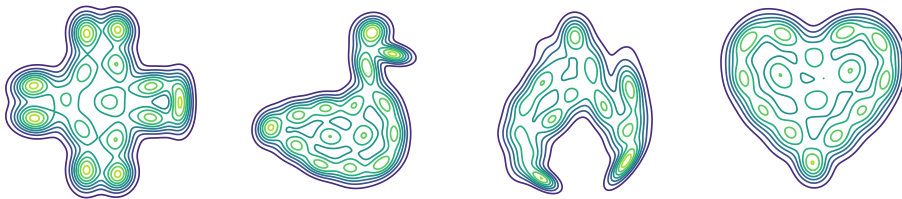


Figure 23: Four GMMs of which we will compute barycentres in [Fig. 24](#).



Figure 24: GMM barycentres between the four corner GMMs computed with the fixed-point solver with  $n = 15$  components. The GMMs are represented by the contours of their densities on  $\mathbb{R}^2$ .

## 5.8 Colour Transfer on a Barycentre of Colour Distributions

In this final experiment, we consider a colour transfer problem. The goal is to compute the barycentre of the colour distributions of several (here three) source images, some of which contain outlier colours, and then use this barycentre as a target measure to modify the colours of a new image (referred to as the *input* here). Figure 25 shows the source images, the *input* image, and the same *input* image after transferring its colour distribution to that of the colour barycentre of the source images. The barycentre is computed either for a  $W_1$  cost or for a  $W_2^2$  cost. This transfer is evaluated on downsampled images, with the RGB matching of a colour  $c$  in the high-resolution image subsequently chosen as  $c + \tau$ , where  $\tau$  is the colour translation obtained for the closest colour to  $c$  in the downsampled image (this amounts to viewing the matching as a piecewise constant translation field). Figure 26 shows the colour distributions of the images in the RGB space. We observe that the  $W_1$  cost enjoys greater robustness to the colour outliers compared to the usual  $W_2^2$  cost.

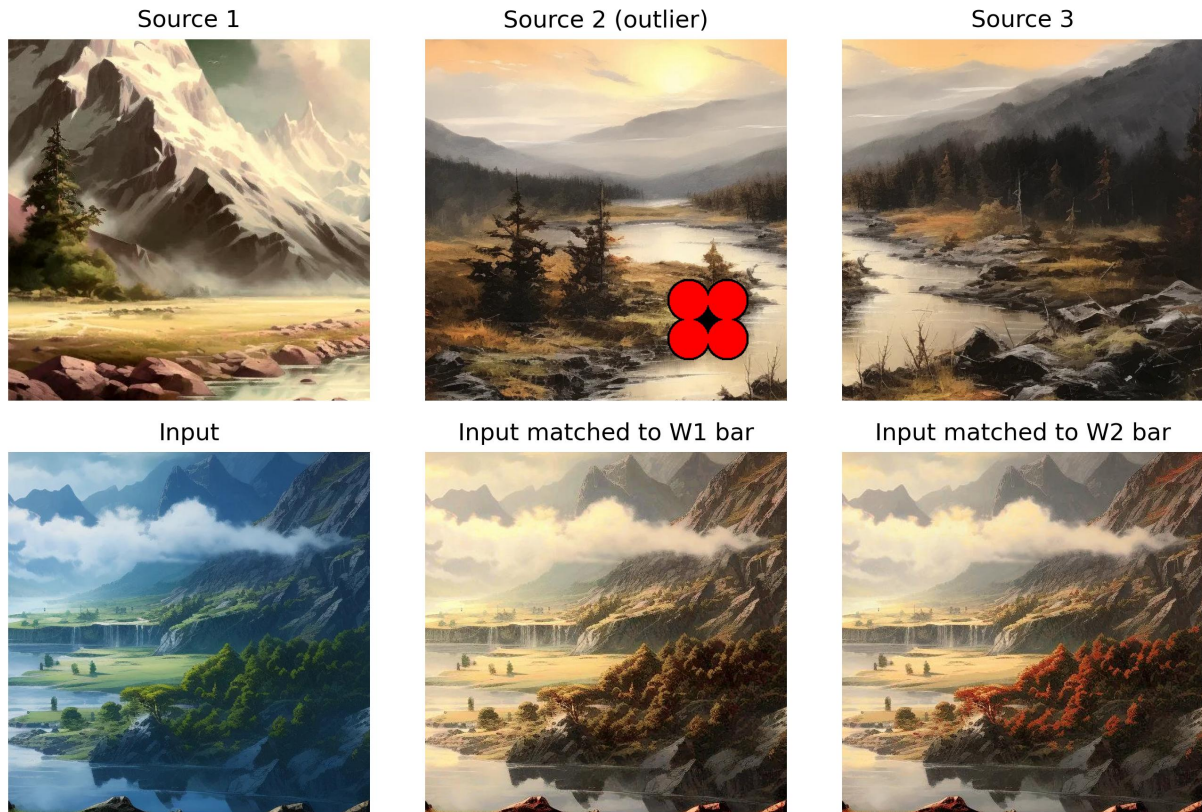


Figure 25: Colour transfer applied to the input image towards the colour barycentre of the source images, for the costs  $W_1$  and  $W_2^2$ . One of the source images contains unwanted colour artifacts, which we see as outliers.

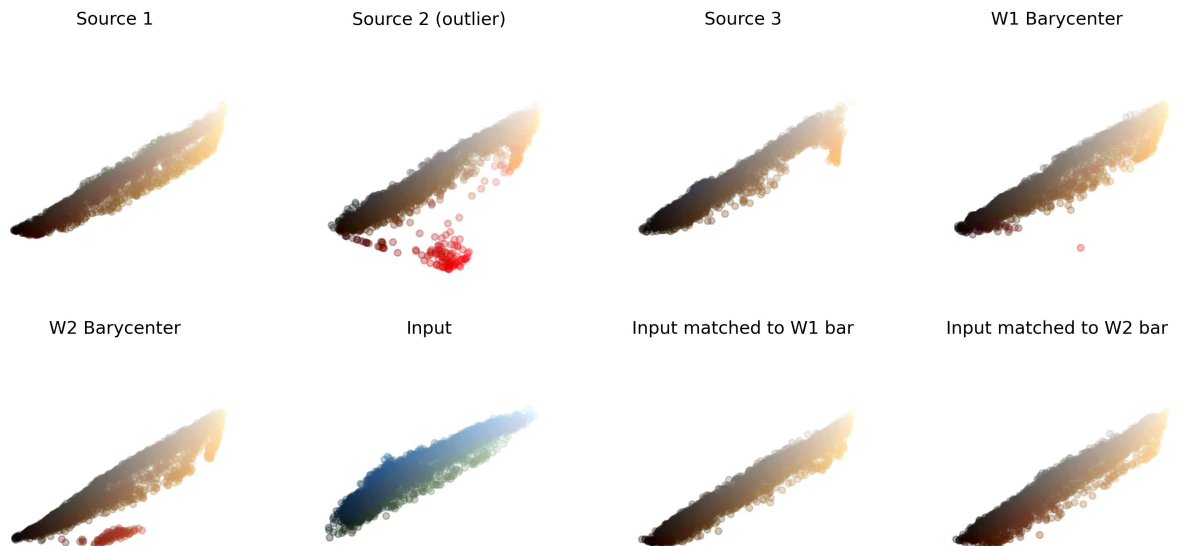


Figure 26: Colour distributions of the different images from figure 25 as well as the  $W_2^2$  and  $W_1$  barycentres of the source images.

## Future Directions

There are numerous directions for future research. To begin with, in [Theorem 3.11](#), we show subsequential convergence to fixed-points of  $G$ , which may not be barycentres. In cases where

barycentres and fixed points may not be unique such as the discrete setting, it remains unclear if there exists fixed points that are not barycentres.

The barycentric fixed-point algorithm (iterating Eq. (21)) has no theoretical guarantees of convergence. Given its computational advantages and its current use in practice for the squared Euclidean cost ([CD14; Fla+21]), this is a timely question.

In Section 3.3, we required a notion of barycentric projection for couplings  $\pi \in \Pi_{c_k}^*(\mu, \nu_k)$ . In  $\mathbb{R}^d$ , the underlying convex combinations are performed using the usual linear structure, however this does not generalise to arbitrary metric spaces. To consider these object more formally on generic (compact) metric spaces, it would be necessary to discuss in more detail the meaning of expectation in a space without a linear structure.

Throughout this work, we relied heavily on Assumption 2, but in practice this can be difficult to verify for costs  $c_k$ : beyond the case  $c_k = h(x-y)$  with  $h$  strictly convex, it is difficult to provide large classes of costs that yield this property on  $B$  (other examples include  $c_k(x, y) = \|P_k x - y\|_2^2$  as in [DGS21] or  $W_2^2$  for absolutely continuous measures). One could alternatively investigate a theoretical framework where  $B$  is a multi-function.

In the absolutely continuous case, the Twist condition can ensure uniqueness of the barycentre, as explained in Remark 2.1. A natural question concerns almost-sure uniqueness in the discrete case, as was partially explored in Section 4.3.

From a numerical standpoint, it has been observed that the fixed-point algorithm converges in very few iterations. A theoretical work extending the discrete Wasserstein case from [Lin23] would bridge a significant gap between theory and practical observation.

## Acknowledgements

We would like to thank Christophe Gaillac for the initial discussions that motivated the introduction of barycentres with generic costs. We thank Nicolas Juillet for useful discussions about the fixed points of the functionals  $G$  and  $H$ . This research was funded in part by the Agence nationale de la recherche (ANR), Grant ANR-23-CE40-0017 and by the France 2030 program, with the reference ANR-23-PEIA-0004.

## References

- [AC11] Martial Agueh and Guillaume Carlier. “Barycenters in the Wasserstein Space”. In: *SIAM Journal on Mathematical Analysis* 43.2 (2011), pp. 904–924. eprint: <https://doi.org/10.1137/100805741>.
- [AC17] Martial Agueh and Guillaume Carlier. “Vers un théorème de la limite centrale dans l’espace de Wasserstein?” In: *Comptes Rendus. Mathématique* 355.7 (2017), pp. 812–818.
- [AB94] Charalambos D. Aliprantis and Kim C. Border. “Correspondences”. In: *Infinite Dimensional Analysis: A Hitchhiker’s Guide*. Berlin, Heidelberg: Springer Berlin Heidelberg, 1994, pp. 458–520.
- [Alt+21] Jason Altschuler, Sinho Chewi, Patrik R Gerber, and Austin Stromme. “Averaging on the Bures-Wasserstein manifold: dimension-free convergence of gradient descent”. In: *Advances in Neural Information Processing Systems* 34 (2021), pp. 22132–22145.
- [AB21] Jason M. Altschuler and Enric Boix-Adsera. *Wasserstein barycenters are NP-hard to compute*. 2021.

- [Álv+16] Pedro C Álvarez-Esteban, E Del Barrio, JA Cuesta-Albertos, and C Matrán. “A fixed-point approach to barycenters in Wasserstein space”. In: *Journal of Mathematical Analysis and Applications* 441.2 (2016), pp. 744–762.
- [ABM16] Ethan Anderes, Steffen Borgwardt, and Jacob Miller. “Discrete Wasserstein barycenters: Optimal transport for discrete data”. In: *Mathematical Methods of Operations Research* 84 (2016), pp. 389–409.
- [Bac+22] Julio Backhoff-Veraguas, Joaquin Fontbona, Gonzalo Rios, and Felipe Tobar. “Bayesian learning with Wasserstein barycenters”. In: *ESAIM: Probability and Statistics* 26 (2022), pp. 436–472.
- [BB25] Florian Beier and Robert Beinert. “Tangential fixpoint iterations for Gromov–Wasserstein barycenters”. In: *SIAM Journal on Imaging Sciences* 18.2 (2025), pp. 1058–1100.
- [BBS23] Florian Beier, Robert Beinert, and Gabriele Steidl. *Multi-Marginal Gromov-Wasserstein Transport and Barycenters*. 2023. arXiv: [2205.06725](https://arxiv.org/abs/2205.06725) [math.OC].
- [Ben+15] Jean-David Benamou, Guillaume Carlier, Marco Cuturi, Luca Nenna, and Gabriel Peyré. “Iterative Bregman projections for regularized transportation problems”. In: *SIAM Journal on Scientific Computing* 37.2 (2015), A1111–A1138.
- [BJL17] Rajendra Bhatia, Tanvi Jain, and Yongdo Lim. “On the Bures-Wasserstein distance between positive definite matrices”. In: *arXiv* (Dec. 2017). eprint: [1712.01504](https://arxiv.org/abs/1712.01504).
- [BCP19] Jérémie Bigot, Elsa Cazelles, and Nicolas Papadakis. “Penalization of barycenters in the Wasserstein space”. In: *SIAM Journal on Mathematical Analysis* 51.3 (2019), pp. 2261–2285.
- [BPC16] Nicolas Bonneel, Gabriel Peyré, and Marco Cuturi. “Wasserstein barycentric coordinates: histogram regression using optimal transport.” In: *ACM Trans. Graph.* 35.4 (2016), pp. 71–1.
- [BFR24a] Camilla Brizzi, Gero Friesecke, and Tobias Ried. *h-Wasserstein barycenters*. 2024. arXiv: [2402.13176](https://arxiv.org/abs/2402.13176) [math.AP].
- [BFR24b] Camilla Brizzi, Gero Friesecke, and Tobias Ried. “ $p$ -Wasserstein barycenters”. In: *arXiv preprint arXiv:2405.09381* (2024).
- [CCE24] Guillaume Carlier, Enis Chenchene, and Katharina Eichinger. “Wasserstein Medians: Robustness, PDE Characterization, and Numerics”. In: *SIAM Journal on Mathematical Analysis* 56.5 (2024), pp. 6483–6520.
- [CE10] Guillaume Carlier and Ivar Ekeland. “Matching for teams”. In: *Economic theory* 42 (2010), pp. 397–418.
- [CD14] Marco Cuturi and Arnaud Doucet. “Fast Computation of Wasserstein Barycenters”. In: *Proceedings of the 31st International Conference on Machine Learning*. Ed. by Eric P. Xing and Tony Jebara. Vol. 32. Proceedings of Machine Learning Research. Beijing, China: PMLR, June 2014, pp. 685–693.
- [DD20] Julie Delon and Agnes Desolneux. “A Wasserstein-type distance in the space of Gaussian mixture models”. In: *SIAM Journal on Imaging Sciences* 13.2 (2020), pp. 936–970.
- [DGS21] Julie Delon, Nathaël Gozlan, and Alexandre Saint-Dizier. *Generalized Wasserstein barycenters between probability measures living on different subspaces*. 2021.
- [Fla+21] Rémi Flamary, Nicolas Courty, Alexandre Gramfort, Mokhtar Z. Alaya, Aurélie Boisbunon, Stanislas Chambon, Laetitia Chapel, Adrien Corenflos, Kilian Fatras, Nemo Fournier, Léo Gautheron, Nathalie T.H. Gayraud, Hicham Janati, Alain Rakotomamonjy, Ievgen Redko, Antoine Rolet, Antony Schutz, Vivien Seguy, Danica J. Sutherland, Romain Tavenard, Alexander Tong, and Titouan Vayer.

- “POT: Python Optimal Transport”. In: *Journal of Machine Learning Research* 22.78 (2021), pp. 1–8.
- [Gor+19] Paula Gordaliza, Eustasio Del Barrio, Gamboa Fabrice, and Jean-Michel Loubes. “Obtaining fairness using optimal transport theory”. In: *International conference on machine learning*. PMLR. 2019, pp. 2357–2365.
- [Goz+17] Nathael Gozlan, Cyril Roberto, Paul-Marie Samson, and Prasad Tetali. “Kantorovich duality for general transport costs and applications”. In: *Journal of Functional Analysis* 273.11 (2017), pp. 3327–3405.
- [Ho+17] Nhat Ho, XuanLong Nguyen, Mikhail Yurochkin, Hung Hai Bui, Viet Huynh, and Dinh Phung. “Multilevel clustering via Wasserstein means”. In: *International conference on machine learning*. PMLR. 2017, pp. 1501–1509.
- [KP17] Young-Heon Kim and Brendan Pass. “Wasserstein barycenters over Riemannian manifolds”. In: *Adv. Math.* 307 (2017), pp. 640–683.
- [Kor+22] Alexander Korotin, Vage Egiazarian, Lingxiao Li, and Evgeny Burnaev. “Wasserstein iterative networks for barycenter estimation”. In: *Advances in Neural Information Processing Systems* 35 (2022), pp. 15672–15686.
- [Lin23] Johannes von Lindheim. “Simple approximative algorithms for free-support Wasserstein barycenters”. In: *Computational Optimization and Applications* 85.1 (2023), pp. 213–246.
- [MDC20] Quentin Mérigot, Alex Delalande, and Frederic Chazal. “Quantitative stability of optimal transport maps and linearization of the 2-Wasserstein space”. In: *International Conference on Artificial Intelligence and Statistics*. PMLR. 2020, pp. 3186–3196.
- [Mi+18] Liang Mi, Wen Zhang, Xianfeng Gu, and Yalin Wang. “Variational wasserstein clustering”. In: *Proceedings of the European Conference on Computer Vision (ECCV)*. 2018, pp. 322–337.
- [MM21] Eduardo Fernandes Montesuma and Fred Maurice Ngole Mboula. “Wasserstein barycenter for multi-source domain adaptation”. In: *Proceedings of the IEEE/CVF conference on computer vision and pattern recognition*. 2021, pp. 16785–16793.
- [PC19] G. Peyré and M. Cuturi. “Computational Optimal Transport”. In: *Foundations and Trends in Machine Learning* 51.1 (2019), pp. 1–44.
- [Rab+12] Julien Rabin, Gabriel Peyré, Julie Delon, and Marc Bernot. “Wasserstein barycenter and its application to texture mixing”. In: *Scale Space and Variational Methods in Computer Vision: Third International Conference, SSVM 2011, Ein-Gedi, Israel, May 29–June 2, 2011, Revised Selected Papers 3*. Springer. 2012, pp. 435–446.
- [San15] Filippo Santambrogio. “Optimal transport for applied mathematicians”. In: *Birkhäuser, NY* 55.58-63 (2015), p. 94.
- [Sol+15] Justin Solomon, Fernando De Goes, Gabriel Peyré, Marco Cuturi, Adrian Butscher, Andy Nguyen, Tao Du, and Leonidas Guibas. “Convolutional wasserstein distances: Efficient optimal transportation on geometric domains”. In: *ACM Transactions on Graphics (ToG)* 34.4 (2015), pp. 1–11.
- [Vil09] Cédric Villani. *Optimal transport : old and new / Cédric Villani*. eng. Grundlehren der mathematischen Wissenschaften. Berlin: Springer, 2009.